To appear in Journal of the Mechanics and Physics of Solids (DOI: 10.1016/j.jmps.2026.106909)

A Transport-Constrained Gradient-Flow Description of Continuum Dislocation Dynamics

Paria Behnoud [1,2,*] Anthony Rollett,[3] Carlos Mora-Corral,[4] and Kaushik Dayal [2,5,6,†]

[1] *Program in Computational Mechanics, Carnegie Mellon University*
[2] *Department of Civil and Environmental Engineering, Carnegie Mellon University*
[3] *Department of Materials Science and Engineering, Carnegie Mellon University*
[4] *Departamento de Matemáticas, Universidad Autónoma de Madrid*
[5] *Center for Nonlinear Analysis, Department of Mathematical Sciences, Carnegie Mellon University*
[6] *Department of Mechanical Engineering, Carnegie Mellon University*

(Dated: November 6, 2026)

Gradient flow frameworks are fundamental to numerous models of defect and microstructure evolution. This work develops a gradient flow formulation for continuum dislocation dynamics, with the key distinction that the admissible rates are transport-constrained. Using the dislocation density and compatible slip fields as the primary state variables, their admissible rates are restricted by geometric conservation laws. The corresponding transport velocities are then selected variationally through a constrained Onsager principle. The resulting model has both a variational gradient flow structure and consistency with the geometric dislocation conservation statement; existing models of dislocation evolution typically have either one or the other feature.

This thermodynamic structure provides a dislocation driving force that includes elastic stress contributions – corresponding to the classical Peach–Koehler force – as well as contributions from the core and nonconvex lattice energies. A simplified version of the model is used to study the energetics and dynamics of an opposite-sign dislocation pair. The lattice energy keeps the cores compact, and an external applied shear either assists annihilation or, above a threshold, separates the pair.

1. Introduction

Dislocation evolution is a central problem in the mechanics of crystalline solids. The motion, interaction, and collective organization of dislocations govern plastic deformation, strain hardening, size effects, and the emergence of microstructure. A fundamental goal is therefore to formulate dislocation dynamics from principles of energy, dissipation, and kinematics, e.g., [McD24, KCO02].

Variational principles, such as gradient flows, have played a central role in continuum theories of materials evolution, e.g., [CTC97, MO08, PF90], and established this viewpoint as a powerful framework for describing dissipative evolution in materials. For example, in models of grain-boundary motion [KL01, KLL$^+$04], the evolution law is often obtained by combining a free energy with an appropriate dissipation mechanism or metric structure. More generally, Onsager-type variational principles provide a systematic way to combine thermodynamic driving forces with dissipation mechanisms [Ons31, Doi11]. In such approaches, the choice of free energy, together with the gradient-flow metric, dissipation mechanism, and admissible class of variations, determines the dissipative evolution.

Dislocation mechanics presents an important and interesting setting for this framework. The elastic energy depends on the elastic distortion, while the defect content is encoded by the incompatibility of the plastic distortion. Thus the energetic driving force is tied to both elastic equilibrium and the geometry of dislocations. However, the evolution of dislocations cannot be described by arbitrary changes of the plastic distortion: dislocations move by transport, and their admissible evolution must respect the conservation and compatibility structure associated with the dislocation density tensor [Mur63].

This provides the motivation for the present work: to formulate a variational principle in which the motion is driven by energy and dissipation, but the admissible directions are constrained by dislocation transport. The central question is how to construct a gradient-flow-type theory for dislocations in which the velocity of transport, rather than an arbitrary rate of plastic distortion, is selected by a variational principle.

1.A. Prior Approaches to Dislocation Evolution

Variational perspectives and related thermodynamic approaches have played a key role in the formulation of models of dislocation dynamics, and plasticity broadly. An early work was by Rickman and Viñals [RV97], who developed a related coarse-grained dissipative model in which the dislocation-density tensor evolves according to Burgers-vector conservation and a phenomenological flux chosen to decrease the plastic free energy. Koslowski, Cuitiño, and Ortiz [KCO02] developed a phase-field model with gradient-flow dynamics for dislocation evolution, incorporating long-range elastic interactions and core effects. Gurtin [Gur04] developed a gradient theory of small-deformation plasticity based on virtual power and microforce balance, in which the free energy depends on the elastic response and on the Burgers tensor, or equivalently on the curl of the plastic distortion. Cermelli and

* pbehnoud@cmu.edu
† Kaushik.Dayal@cmu.edu

Gurtin [CG99] used maximal dissipation to deduce the dynamics of dislocations, which was then analyzed mathematically by Blass et al. [BFLM15] and Alicandro et al. [ALGP16]. More recently, Dondl, Kurzke, and Wojtowytsch [DKW18] studied the gradient flow of a phase-field model for plastic slip in the presence of forest dislocations and showed that the limiting dynamics may differ from the gradient flow of the limiting energy, with the obstacles generating an effective frictional resistance.

Continuum dislocation dynamics has also emphasized the transport character of dislocation evolution. The transport viewpoint underlying continuum dislocation dynamics has its origins in the conservation laws for Burgers-vector density and dislocation flux introduced by Kosevich [Kos62] and the transport law for the dislocation density tensor introduced by Mura [Mur63, Mur13]. These seminal kinematic structures provide the starting point for many subsequent continuum descriptions of dislocation evolution. Modern continuum dislocation dynamics formulations further emphasize the role of transport, closure assumptions, and mobility laws in connecting dislocation density evolution to crystal plasticity [HSZG14, EAP20].

Many continuum theories build on this transport structure but close the model by prescribing the velocity or current through an additional constitutive kinetic law, with some key references cited below. Groma and Balogh [GB99] derived transport equations for positive and negative edge dislocation densities starting from overdamped equations of motion for discrete dislocations. Limkumnerd and Sethna developed a continuum theory in which the Nye dislocation density tensor evolves through a topological current derived from Peach–Koehler-driven glide, and demonstrated the formation of sharp dislocation walls [LS06, LS07, LS08]. Chen et al. [CCP$^+$13] developed a three-dimensional scaling theory of continuum dislocation dynamics leading to self-organized fractal pattern formation. Hochrainer, Zaiser, and Gumbsch [HZG07] introduced higher-dimensional continuum dislocation dynamics to represent curved dislocation lines, with velocities determined by Peach–Koehler forces, mobility laws, and possible line-tension terms. Monavari and Zaiser [MZ18] formulated a slip-system-specific form of the dislocation transport law in which the glide direction is fixed kinematically, while the scalar velocity is supplied constitutively. Sandfeld and Zaiser [SZ15] developed a minimal continuum dislocation plasticity model involving total density, geometrically necessary dislocation density, and curvature density, closed by a thresholded mobility law. Xia and El-Azab [XEA15] used an explicit evolution law based on the dislocation transport law and prescribed the scalar speed through a linear mobility relation involving the resolved shear stress. More recently, Zhang, Wu, and Zaiser [ZWZ25] reformulated continuum dislocation dynamics as a phase-field theory with conserved order parameters and applied it to dislocation patterning. A related class of approaches represents individual dislocation lines through evolving level-set functions: e.g., Chen et al. [CCS$^+$10] developed a three-dimensional level-set formulation in which the dislocation motion is overdamped and the velocity is prescribed through a mobility tensor with distinct glide and climb components acting on a Peach–Koehler force. The total driving stress includes self-stress, applied stress, and stresses generated by misfitting obstacles.

At the level of state variables, continuum descriptions have also emphasized the role of geometrically necessary dislocations in size-dependent plasticity. Gao and Huang [GH03] and Arsenlis and Parks [AP99, AP02] developed formulations in which geometrically necessary dislocation content plays an important role in size-dependent plasticity and crystal-plasticity response. This provides a related use of dislocation density as a measure of incompatibility. A complementary approach is due to Rosakis [Ros01], who analyzed dislocations in an augmented continuum model and developed kinetic relations between applied shear stress and dislocation speed, providing a comparison at the level of force–velocity closure.

1.B. Contributions of This Work

The distinguishing feature of the present formulation is that we develop a gradient flow structure for dislocation dynamics that also respects the geometric conservation laws of dislocation transport. Specifically, the dislocation transport law defines the admissible tangent directions of the variational evolution, and the associated transport velocities are selected through a constrained Onsager principle. While there are dislocation evolution models that have a gradient flow structure, they typically do not obey the geometric conservation law of dislocation dynamics; conversely, dislocation dynamics models that are based on the geometric conservation law do not have a gradient-flow structure.

We develop a formulation in which the primary independent state variables are the dislocation density field $\boldsymbol{\alpha}$ and the compatible slip field $\boldsymbol{R}$, with the plastic distortion $\boldsymbol{\beta}_p$ being constructed from $\boldsymbol{\alpha}$ and $\boldsymbol{R}$. The admissible rates of the theory are induced by transport laws: $\boldsymbol{\alpha}$ is transported as a vector-valued two-form, while $\boldsymbol{R}$ is transported row-wise as a vector-valued one-form. Since the transport law for $\boldsymbol{\alpha}$ determines the plastic-distortion rate only up to a gradient, Mura's rate [Mur63] corresponds to setting this gradient to zero; here, it is given instead by the transport of $\boldsymbol{R}$, and Mura's choice is recovered when $\boldsymbol{R}$ is not transported. We use a constrained Onsager principle to select the transport velocities variationally, with the variations taken along the transport-admissible directions. Minimization of the Onsager functional determines the optimal velocities associated with $\boldsymbol{\alpha}$ and $\boldsymbol{R}$, and thereby yields a transport-constrained gradient-flow system.

The distinguishing feature is the organization of the evolution as a gradient flow on the transport-admissible tangent space, with a state-dependent metric determined by the dissipation due to the transport velocities. The Onsager construction identifies a state-dependent metric on the transport-admissible tangent space and interprets the evolution as steepest descent of the reduced free energy with respect to this metric. The variation of the total reduced free energy is restricted to the tangent space generated by transport satisfying the dislocation transport law, and the dissipation potential defines a state-dependent metric on that tangent space. In essence, our formulation replaces the usual thermodynamic force–velocity viewpoint with an explicit metric structure for the admissible evolution. This additional structure provides a natural basis for variational time discretizations and for future

analysis of the metric and well-posedness properties of the evolution.

The resulting driving force for $\boldsymbol{\alpha}$ has the structure of a generalized Peach–Koehler force, with additional thermodynamic contributions generated by the defect (core) energy and nonconvex lattice energy. In the limit in which these additional energetic contributions vanish, the formulation recovers the classical Peach–Koehler force for a single dislocation line. The model therefore embeds the standard force law of dislocation mechanics within the transport-constrained variational framework, with the classical Peach–Koehler closure recovered as a special energetic limit.

Remark 1.1 (Wasserstein gradient flows and their Riemannian formulation)**.** The present construction is closely related in spirit to Wasserstein gradient flows, where dissipative evolution is formulated as the steepest descent of a free energy subject to a transport constraint. The scheme introduced by Jordan, Kinderlehrer, and Otto showed that certain dissipative partial differential equations can be interpreted as gradient flows of free energy with respect to the Wasserstein metric [JKO98]. Otto subsequently developed the formal Riemannian interpretation of such transport gradient flows, in which the continuity equation induces a metric structure on admissible tangent directions [Ott01]. Later developments clarified the analytical and variational structure of Wasserstein gradient flows and their connection to transport, continuity equations, and variational time discretizations [AGS08, San15, San17, Fri24].

The analogy with the present formulation lies in the role of transport in defining admissible tangent directions. In the Wasserstein setting, density rates are generated through a continuity equation and the associated transport velocity. Here, admissible changes of the dislocation density are generated by dislocation velocities through the dislocation transport law, while the compatible slip is evolved through its own transport law. The corresponding metric therefore measures the dissipation required to realize transport-admissible variations rather than arbitrary variations. □

1.C. Structure of the Paper

- Section 2 lays out the kinematics, specifically the relation of the plastic distortion $\boldsymbol{\beta}_p$ to the dislocation density tensor $\boldsymbol{\alpha}$ and the compatible slip $\boldsymbol{R}$, and the free energy for dislocation plasticity.
- Section 3 develops the Lie-derivative interpretation of the defect variables and derives the transport-admissible tangent directions for $\boldsymbol{\alpha}$ and $\boldsymbol{R}$.
- Section 4 formulates the transport-constrained Onsager principle, and derives the corresponding driving forces and the resulting transport equations. It also identifies the associated transport manifold, metric, formal gradient-flow structure, and energy-dissipation identity.
- Section 5 compares the derived driving force on $\boldsymbol{\alpha}$ with the classical Peach–Koehler force. The roles of the lattice energy and the core energy are discussed, and the driving force is shown to reduce to the classical expression in the case of a single straight dislocation when the lattice energy is neglected.
- Section 6 compares the structure of the current with the classical Cahn–Hilliard approach in phase-field modeling of conserved species.
- Section 7 applies the model to the annihilation of two opposite-sign dislocations on a single glide plane. The pair glides toward annihilation, and a superposed uniform resolved shear stress either assists annihilation or, above a threshold, separates the pair.

2. Kinematics and Free Energy Formulation

2.A. Notation

We work in the geometrically linear setting. We use δ to denote a variation, while $D\mathcal{F}[\boldsymbol{z}][\boldsymbol{s}]$ denotes the directional derivative of a functional $\mathcal{F}$ at a generic state $\boldsymbol{z}$ in the direction $\boldsymbol{s}$. We use the Einstein convention that repeated indices are summed unless otherwise stated. Throughout the paper, we assume that all functions have sufficient regularity for all operations being performed to be well defined.

2.B. Kinematics

The body Ω is a bounded, smooth, simply connected[1] domain with connected boundary $\partial\Omega$ and outward unit normal $\boldsymbol{n}$; curl, divergence, gradient, and cross products act row-wise. The state variables are the displacement $\boldsymbol{u}$, the dislocation density tensor $\boldsymbol{\alpha}$, and the compatible slip $\boldsymbol{R}$, subject to

$$\operatorname{div}\boldsymbol{\alpha} = \boldsymbol{0}, \qquad \operatorname{curl}\boldsymbol{R} = \boldsymbol{0} \quad \text{in } \Omega. \tag{2.1}$$

Since Ω is simply connected, $\boldsymbol{R} = \nabla\boldsymbol{A}$ for a field $\boldsymbol{A}$ determined up to a constant [Yav13].

---

[1] The case of dislocations in non-simply-connected domains is studied in [YG12, SY23].

Following the Stokes–Helmholtz decomposition in dislocation mechanics [Krö58, Krö10, Wen98, BSW01], we define the plastic distortion

$$\boldsymbol{\beta}_p := \mathcal{C}[\boldsymbol{\alpha}] + \boldsymbol{R}, \quad \text{where} \quad \mathcal{C}[\boldsymbol{\alpha}](\boldsymbol{x}) := \operatorname{curl} \int_\Omega \boldsymbol{G}(\boldsymbol{x},\boldsymbol{y})\,\boldsymbol{\alpha}(\boldsymbol{y})\,\mathrm{d}\Omega_{\boldsymbol{y}} \tag{2.2}$$

and $\boldsymbol{G}$ is the Green's function of the vector Laplacian in Ω, applied to each row of $\boldsymbol{\alpha}$, with the boundary conditions below. That is, $\boldsymbol{H} := \displaystyle\int_\Omega \boldsymbol{G}\,\boldsymbol{\alpha}\,\mathrm{d}\Omega_{\boldsymbol{y}}$ solves

$$-\Delta \boldsymbol{H} = \boldsymbol{\alpha} \quad \text{in } \Omega, \qquad \boldsymbol{H}\times\boldsymbol{n} = \boldsymbol{0}, \quad \operatorname{div}\boldsymbol{H} = \boldsymbol{0} \quad \text{on } \partial\Omega, \tag{2.3}$$

which has exactly one solution because $\partial\Omega$ is connected [ABDG98]. By (2.1), $\operatorname{div}\boldsymbol{H}$ is harmonic in Ω and vanishes on $\partial\Omega$, so $\operatorname{div}\boldsymbol{H} = \boldsymbol{0}$ and $\operatorname{curl}\operatorname{curl}\boldsymbol{H} = -\Delta\boldsymbol{H} = \boldsymbol{\alpha}$. Hence $\mathcal{C}[\boldsymbol{\alpha}] = \operatorname{curl}\boldsymbol{H}$ satisfies

$$\operatorname{curl}\mathcal{C}[\boldsymbol{\alpha}] = \boldsymbol{\alpha}, \quad \operatorname{div}\mathcal{C}[\boldsymbol{\alpha}] = \boldsymbol{0} \quad \text{in } \Omega, \qquad \mathcal{C}[\boldsymbol{\alpha}]\boldsymbol{n} = \boldsymbol{0} \quad \text{on } \partial\Omega, \tag{2.4}$$

where the boundary condition follows from $\boldsymbol{H}\times\boldsymbol{n} = \boldsymbol{0}$. The solution of this div–curl problem is unique because Ω is simply connected [ABDG98]. From (2.1)–(2.4),

$$\operatorname{curl}\boldsymbol{\beta}_p = \boldsymbol{\alpha}, \tag{2.5}$$

so $\boldsymbol{\alpha}$ is the dislocation density of $\boldsymbol{\beta}_p$. The field $\mathcal{C}[\boldsymbol{\alpha}]$ is the incompatible part of $\boldsymbol{\beta}_p$, determined nonlocally by $\boldsymbol{\alpha}$, and $\boldsymbol{R}$ is its compatible part. Conversely, every $\boldsymbol{\beta}_p$ has exactly one such decomposition, with $\boldsymbol{\alpha} = \operatorname{curl}\boldsymbol{\beta}_p$ and $\boldsymbol{R} = \boldsymbol{\beta}_p - \mathcal{C}[\operatorname{curl}\boldsymbol{\beta}_p]$.

The displacement gradient decomposes additively as

$$\nabla\boldsymbol{u} = \boldsymbol{\beta}_e + \boldsymbol{\beta}_p, \tag{2.6}$$

which defines the elastic distortion $\boldsymbol{\beta}_e$.

Figure 1 schematically illustrates a simple-shear example of the compatible part $\boldsymbol{R} = \nabla\boldsymbol{A}$.

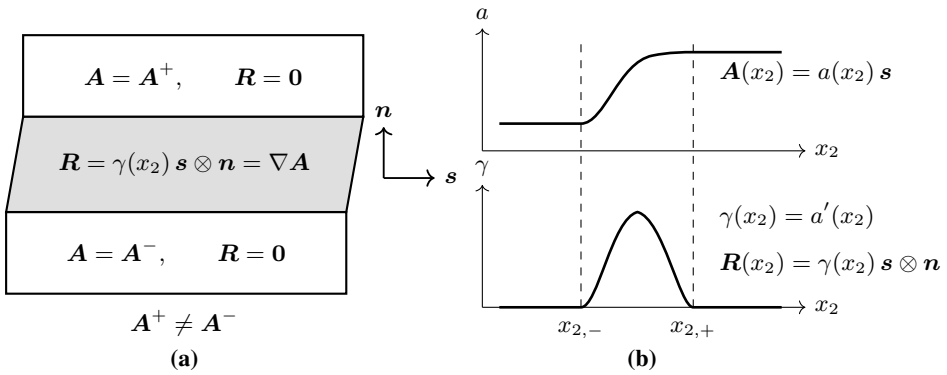


Figure 1. Schematic example of a compatible slip through simple shear, showing plastic slip and nonzero $\boldsymbol{\beta}_p$ without the presence of dislocations. The compatible part of the plastic distortion is represented by $\boldsymbol{R} = \nabla\boldsymbol{A}$. In (a), $\boldsymbol{A}$ is constant outside the shaded layer and varies within it. As an illustrative example, we take $\boldsymbol{A}(x_2) = a(x_2)\,\boldsymbol{s}$, where $\boldsymbol{s}$ denotes the slip direction and $\boldsymbol{n}$ the layer normal. It follows that $\boldsymbol{R} = \gamma(x_2)\,\boldsymbol{s}\otimes\boldsymbol{n}$, with $\gamma(x_2) = a'(x_2)$, so that $\boldsymbol{R}$ vanishes outside the layer and is localized within it. In (b), we see the corresponding one-dimensional profiles.

2.B.1. Boundary Conditions

The boundary $\partial\Omega$ consists of disjoint parts $\partial\Omega_D$ and $\partial\Omega_N$, on which the displacement $\bar{\boldsymbol{u}}$ and the traction $\bar{\boldsymbol{t}}$ are prescribed:

$$\boldsymbol{u} = \bar{\boldsymbol{u}} \quad \text{on } \partial\Omega_D, \qquad \boldsymbol{\sigma}^*\boldsymbol{n} = \bar{\boldsymbol{t}} \quad \text{on } \partial\Omega_N, \tag{2.7}$$

where $\boldsymbol{\sigma}^*$ is the stress (2.14). If $\partial\Omega_D$ is empty, the applied tractions have zero net force and moment. On $\partial\Omega$, we further impose, for the transport velocities $\boldsymbol{V}_{\boldsymbol{\alpha}}$ and $\boldsymbol{V}_R$ of Section 3,

$$\boldsymbol{R}\boldsymbol{V}_R = \boldsymbol{0}, \qquad \boldsymbol{P}_R^{\mathrm{d}}\boldsymbol{n} = \boldsymbol{0}, \tag{2.8}$$

and either $(\boldsymbol{\alpha} \times \boldsymbol{V}_{\boldsymbol{\alpha}}) \times \boldsymbol{n} = \boldsymbol{0}$ or $\boldsymbol{P}_{\alpha}^{\mathrm{d}} \times \boldsymbol{n} = \boldsymbol{0}$ (microscopically hard or free [Gur04]), where $\boldsymbol{P}_{\alpha}^{\mathrm{d}}$ and $\boldsymbol{P}_{R}^{\mathrm{d}}$ are defined in (2.12). In Section 6, $\boldsymbol{J} \cdot \boldsymbol{n} = 0$ on $\partial\Omega$. Under these conditions, all boundary terms arising from integration by parts vanish. Surface energies, such as those of the steps left where dislocations exit the body, are not included.

2.C. Energetics

We use the general free energy:

$$\mathcal{F}[\boldsymbol{u}, \boldsymbol{\alpha}, \boldsymbol{R}] := \int_{\Omega} W_e\left(\nabla \boldsymbol{u} - \boldsymbol{\beta}_p\right) \,\mathrm{d}\Omega + \int_{\Omega} W_{\alpha}\left(\boldsymbol{\alpha}\right) \,\mathrm{d}\Omega + \int_{\Omega} W_R\left(\nabla \boldsymbol{R}\right) \,\mathrm{d}\Omega + \int_{\Omega} \Psi\left(\boldsymbol{\beta}_p\right) \,\mathrm{d}\Omega - \int_{\partial\Omega_N} \bar{\boldsymbol{t}} \cdot \boldsymbol{u} \,\mathrm{d}\Gamma, \tag{2.9}$$

where the plastic distortion is reconstructed according to (2.2), $\boldsymbol{\beta}_p = \mathcal{C}[\boldsymbol{\alpha}] + \boldsymbol{R}$. Here, the terms W_e, W_{α}, W_R, and Ψ are stored-energy densities; dissipation is represented by the velocity-dependent terms in the Onsager functional (4.4).

For simplicity, the elastic energy density $W_e(\boldsymbol{\beta}_e)$ is taken to have the quadratic form:

$$W_e\left(\nabla \boldsymbol{u} - \boldsymbol{\beta}_p\right) := \frac{1}{2}\left(\nabla \boldsymbol{u} - \boldsymbol{\beta}_p\right) : \boldsymbol{C}\left(\nabla \boldsymbol{u} - \boldsymbol{\beta}_p\right), \tag{2.10}$$

where $\boldsymbol{C}$ is the fourth-order elasticity tensor. The corresponding stress is then defined as:

$$\boldsymbol{\sigma} := \boldsymbol{C}\boldsymbol{\beta}_e = \boldsymbol{C}\left(\nabla \boldsymbol{u} - \boldsymbol{\beta}_p\right) = \boldsymbol{C}\left(\nabla \boldsymbol{u} - \mathcal{C}[\boldsymbol{\alpha}] - \boldsymbol{R}\right). \tag{2.11}$$

The defect-energy density $W_{\alpha}(\boldsymbol{\alpha})$ is a function of the dislocation density and represents the dislocation core energy. Core regularization and dislocation-density-dependent energetic effects have entered continuum dislocation theories through several distinct routes. In nonsingular continuum models of dislocations, the dislocation core is spatially regularized, removing the classical elastic singularity while retaining a Peach–Koehler-type force evaluated from the regularized stress field [CAWB06, LM05, Laz13, PLAG18, AL17]. Defect or core energy contributions have been naturally introduced through free energy densities that are functions of the dislocation density tensor, e.g. [Gur04].

The lattice-energy density $\Psi(\boldsymbol{\beta}_p)$ is a nonconvex function representing crystallographic slip resistance relative to a prescribed reference lattice [Cla11, EE07]. We assume $\Psi(\boldsymbol{\beta}_p + \boldsymbol{S}) = \Psi(\boldsymbol{\beta}_p)$ for the prescribed lattice-equivalent slip increments $\boldsymbol{S}$ [Eri80, PZ03]; under a change of global reference configuration, the lattice symmetries must be transformed consistently. Similar Peierls-type nonconvex lattice energies have been used to represent crystallographic slip in several prior models [KCO02, WJCK01, RLBF03, SW04, HBGK11, PMB$^+$20, Ros01, RV13].

Finally, $W_R(\nabla \boldsymbol{R})$ is an energy associated with spatial gradients of the compatible slip $\boldsymbol{R}$. For standard models of dislocation plasticity, *this contribution vanishes*, i.e., $W_R \equiv 0$. However, we retain it in the model for generality as it can be used to represent phase transformations when these are coupled to dislocation plasticity.

Free energies containing these, or closely related, energetic elements have appeared in continuum, gradient, and phase-field descriptions of dislocations. In particular, elastic energies coupled to the Burgers tensor or dislocation density have been considered in continuum dislocation plasticity models, e.g., [Gur04, GCZ03, Zai15, Hoc16].

Remark 2.1 (Contribution of the Compatible Slip to the Energy)**.** The compatible slip contributes to the plastic distortion $\boldsymbol{\beta}_p = \mathcal{C}[\boldsymbol{\alpha}] + \boldsymbol{R}$, and hence to the free energy through the elastic energy W_e and the lattice energy Ψ, regardless of whether the additional regularization term W_R is retained. □

For later use, we define the energy-conjugate quantities:

$$\boldsymbol{P}_{\alpha}^{\mathrm{d}} := \frac{\partial W_{\alpha}}{\partial \boldsymbol{\alpha}}, \qquad \boldsymbol{P}_{R}^{d} := \frac{\partial W_R}{\partial \nabla \boldsymbol{R}}, \qquad \boldsymbol{P}_{\Psi} := \frac{\partial \Psi}{\partial \boldsymbol{\beta}_p}. \tag{2.12}$$

2.C.1. Reduced Energy by Minimizing out the Displacement

For fixed $(\boldsymbol{\alpha}, \boldsymbol{R})$, the displacement field $\boldsymbol{u}^*$ is determined by minimizing the free energy with respect to $\boldsymbol{u}$. This reflects the physical statement that we expect mechanical equilibrium to be achieved much faster than the scale of defect relaxation. Therefore, we are essentially at mechanical equilibrium[2] at all times as the defect density evolves.

The equilibrium displacement $\boldsymbol{u}^*[\boldsymbol{\alpha}, \boldsymbol{R}]$ is obtained as the solution of:

$$\operatorname{div} \boldsymbol{\sigma}^* = \boldsymbol{0}, \text{ in } \Omega, \tag{2.13a}$$

$$\boldsymbol{\sigma}^* \boldsymbol{n} = \bar{\boldsymbol{t}}, \text{ on } \partial\Omega_N, \tag{2.13b}$$

$$\boldsymbol{u}^* = \bar{\boldsymbol{u}}, \text{ on } \partial\Omega_D, \tag{2.13c}$$

[2] In regimes where inertia is accounted for, the equation of momentum balance does not follow from a minimum principle. However, it is possible – in principle – to eliminate the displacement using momentum balance, and then apply a minimum principle for defect evolution.

where:

$$\boldsymbol{\sigma}^* := \left.\frac{\partial W_e}{\partial \nabla \boldsymbol{u}}\right|_{\boldsymbol{u}^*}. \tag{2.14}$$

Eliminating the displacement field through elastic equilibrium defines the reduced free energy

$$\mathcal{F}^{\mathrm{red}}[\boldsymbol{\alpha}, \boldsymbol{R}] := \mathcal{F}[\boldsymbol{u}^*, \boldsymbol{\alpha}, \boldsymbol{R}]. \tag{2.15}$$

3. Defect Transport Laws through Lie Derivatives

We now describe the geometric origin of the transport constraints: we write transport laws for $\boldsymbol{\alpha}$ and $\boldsymbol{R}$, and the admissible rate for $\boldsymbol{\beta}_p$ is induced using (2.2). We use a Lie-derivative approach that provides a common framework for transporting both $\boldsymbol{\alpha}$ and the compatible slip $\boldsymbol{R}$. It also connects naturally to the transport structure of Wasserstein gradient flows.

3.A. Lie Derivative for Dislocation Density

Following Hochrainer et al [HZG07], we outline the dislocation transport law for α using Lie derivatives. The dislocation density tensor is a vector-valued two-form that measures Burgers-vector content through oriented surface elements:

$$\boldsymbol{\alpha} = \frac{1}{2}\alpha^a{}_{ij}\, \boldsymbol{e}_a \otimes \mathrm{d}x^i \wedge \mathrm{d}x^j. \tag{3.1}$$

For a differential form $\boldsymbol{\omega}$, Cartan's formula gives

$$\mathcal{L}_{\boldsymbol{V}}\boldsymbol{\omega} = \mathrm{d}\left(\iota_{\boldsymbol{V}}\boldsymbol{\omega}\right) + \iota_{\boldsymbol{V}}\left(\mathrm{d}\boldsymbol{\omega}\right), \tag{3.2}$$

where $\iota_{\boldsymbol{V}}$ denotes contraction with the vector field $\boldsymbol{V}$. Applying this to $\boldsymbol{\alpha}$, transported by the dislocation velocity $\boldsymbol{v}$, gives

$$\mathcal{L}_{\boldsymbol{v}}\boldsymbol{\alpha} = \mathrm{d}\left(\iota_{\boldsymbol{v}}\boldsymbol{\alpha}\right) + \iota_{\boldsymbol{v}}\left(\mathrm{d}\boldsymbol{\alpha}\right). \tag{3.3}$$

Since $\boldsymbol{\alpha} = \mathrm{d}\boldsymbol{\beta}_p$, we have

$$\mathrm{d}\boldsymbol{\alpha} = \mathrm{d}^2\boldsymbol{\beta}_p = \boldsymbol{0} \iff \operatorname{div}\boldsymbol{\alpha} = \boldsymbol{0}, \tag{3.4}$$

expressing the fact that dislocation lines cannot end inside the body.

Under the standard identification $\alpha^a{}_{ij} = \epsilon_{ijk}\alpha^a_k$, with ϵ_{ijk} the permutation symbol, the contraction is

$$\iota_{\boldsymbol{v}}\boldsymbol{\alpha} = \boldsymbol{\alpha} \times \boldsymbol{v}, \tag{3.5}$$

where the cross product is row-wise: $\left(\boldsymbol{\alpha} \times \boldsymbol{v}\right)_i = \boldsymbol{\alpha}_i \times \boldsymbol{v}$. We write the transport in terms of $\boldsymbol{V}_{\boldsymbol{\alpha}} := -\boldsymbol{v}$, the negative of the dislocation velocity, which gives the form of the transport law used throughout this paper. Thus

$$\mathcal{L}_{\boldsymbol{v}}\boldsymbol{\alpha} = \operatorname{curl}\left(\boldsymbol{\alpha} \times \boldsymbol{v}\right) = -\operatorname{curl}\left(\boldsymbol{\alpha} \times \boldsymbol{V}_{\boldsymbol{\alpha}}\right). \tag{3.6}$$

The Lie-transport equation provides the classical dislocation transport law of Kosevich and Mura [Kos62, Mur63, Mur13]:

$$\frac{\partial \boldsymbol{\alpha}}{\partial t} + \mathcal{L}_{\boldsymbol{v}}\boldsymbol{\alpha} = \boldsymbol{0} \iff \dot{\boldsymbol{\alpha}} = \operatorname{curl}\left(\boldsymbol{\alpha} \times \boldsymbol{V}_{\boldsymbol{\alpha}}\right). \tag{3.7}$$

This gives the admissible tangent direction for $\boldsymbol{\alpha}$. We define the associated dislocation flux as $\boldsymbol{J}_\alpha := \boldsymbol{\alpha} \times \boldsymbol{V}_{\boldsymbol{\alpha}}$, so that $\dot{\boldsymbol{\alpha}} = \operatorname{curl}\boldsymbol{J}_\alpha$.

3.B. Transport of the Compatible Slip

The geometric viewpoint used here is motivated by transport-based formulations of microstructural evolution, in which the relevant geometric object is evolved through an appropriate transport or conservation law; see, for example, the interface-density balance formulation of Agrawal and Dayal [AD15a, AD15b]. In their setting, the gradient of a phase field is evolved through a conservation statement for interfaces. Here, we adopt the same transport-based viewpoint for $\boldsymbol{R}$, which is evolved directly as a state variable.

Accordingly, we transport $\boldsymbol{R}$ row-wise as a vector-valued one-form. Let $\boldsymbol{V}_R$ denote the velocity field associated with the transport of $\boldsymbol{R}$; in Figure 1, this would correspond to the vertical motion of the slip surfaces as interfaces[3].

---

[3] Under an applied shear, it is possible – though typically unlikely – that the shear is accommodated through the coherent interfacial motion of slip surfaces, but is

Since $\boldsymbol{R} = \nabla \boldsymbol{A}$, each row of $\boldsymbol{R}$ is a closed one-form. Hence, by Cartan's formula,

$$\mathcal{L}_{\boldsymbol{V}_R} \boldsymbol{R} = \mathrm{d}\left(\iota_{\boldsymbol{V}_R} \boldsymbol{R}\right). \tag{3.8}$$

In components,

$$\left(\mathcal{L}_{\boldsymbol{V}_R} \boldsymbol{R}\right)_{ij} = V_R^k \partial_k R_{ij} + R_{ik} \partial_j V_R^k = \partial_j \left(R_{ik} V_R^k\right), \tag{3.9}$$

where the last equality uses $\partial_k R_{ij} = \partial_j R_{ik}$, which follows from $\operatorname{curl} \boldsymbol{R} = \boldsymbol{0}$. Dislocation motion also generates compatible slip, e.g., the slip left behind a gliding dislocation. The evolution equation for the compatible slip is therefore

$$\frac{\partial \boldsymbol{R}}{\partial t} + \mathcal{L}_{\boldsymbol{V}_R} \boldsymbol{R} = \mathcal{P}[\boldsymbol{\alpha} \times \boldsymbol{V}_{\boldsymbol{\alpha}}], \tag{3.10}$$

or equivalently,

$$\dot{R}_{ij} = \left(\mathcal{P}[\boldsymbol{\alpha} \times \boldsymbol{V}_{\boldsymbol{\alpha}}]\right)_{ij} - \partial_j \left(R_{ik} V_R^k\right), \tag{3.11}$$

where, for a field $\boldsymbol{X}$, $\mathcal{P}[\boldsymbol{X}] := \nabla \boldsymbol{w}$, and $\boldsymbol{w}$, determined up to a constant, solves row-wise

$$\varDelta \boldsymbol{w} = \operatorname{div} \boldsymbol{X} \quad \text{in } \Omega, \qquad (\nabla \boldsymbol{w})\boldsymbol{n} = \boldsymbol{X}\boldsymbol{n} \quad \text{on } \partial\Omega. \tag{3.12}$$

Section 3.C shows that $\mathcal{P}[\boldsymbol{X}]$ is the compatible part of $\boldsymbol{X}$ and derives the source $\mathcal{P}[\boldsymbol{\alpha} \times \boldsymbol{V}_{\boldsymbol{\alpha}}]$. Thus $\boldsymbol{R}$ is transported by $\boldsymbol{V}_R$ and generated by dislocation motion, with the condition $\operatorname{curl} \boldsymbol{R} = \boldsymbol{0}$ preserved by the evolution, since both terms on the right of (3.11) are gradients. This structure is analogous to the gradient-based interface-density balance used by Agrawal and Dayal [AD15a].

3.C. Induced Rate of the Plastic Distortion

The transport equations for $\boldsymbol{\alpha}$ and $\boldsymbol{R}$ induce an admissible rate for the plastic distortion. Using (2.2), differentiation gives

$$\dot{\boldsymbol{\beta}}_p = \mathcal{C}[\dot{\boldsymbol{\alpha}}] + \dot{\boldsymbol{R}}. \tag{3.13}$$

Thus the rate of the plastic distortion has an incompatible part induced by the transport of $\boldsymbol{\alpha}$ and a compatible part carried by $\boldsymbol{R}$.

Using the tangent direction induced by the dislocation transport law (3.7), the first term in (3.13) is a lift of $\dot{\boldsymbol{\alpha}}$ from dislocation-density space to plastic-distortion space. Since $\mathcal{C}$ is linear and independent of time, (2.2) and (3.7) give

$$\begin{aligned} \mathcal{C}[\dot{\boldsymbol{\alpha}}](\boldsymbol{x}) &= \operatorname{curl} \int_\Omega \boldsymbol{G}(\boldsymbol{x}, \boldsymbol{y})\, \dot{\boldsymbol{\alpha}}(\boldsymbol{y})\, \mathrm{d}\Omega_{\boldsymbol{y}} = \operatorname{curl} \int_\Omega \boldsymbol{G}(\boldsymbol{x}, \boldsymbol{y})\, \operatorname{curl}\big(\boldsymbol{\alpha} \times \boldsymbol{V}_{\boldsymbol{\alpha}}\big)(\boldsymbol{y})\, \mathrm{d}\Omega_{\boldsymbol{y}} \\ &= \boldsymbol{\alpha} \times \boldsymbol{V}_{\boldsymbol{\alpha}} - \mathcal{P}[\boldsymbol{\alpha} \times \boldsymbol{V}_{\boldsymbol{\alpha}}], \end{aligned} \tag{3.14}$$

where $\mathcal{P}$ is defined in (3.12). For any $\boldsymbol{X}$, the field $\boldsymbol{X} - \mathcal{P}[\boldsymbol{X}]$ has curl $\operatorname{curl} \boldsymbol{X}$, zero divergence, and zero normal component on $\partial\Omega$, so it is the unique solution of the div–curl problem (2.4) with $\boldsymbol{\alpha}$ replaced by $\operatorname{curl} \boldsymbol{X}$. Hence $\mathcal{C}[\operatorname{curl} \boldsymbol{X}] = \boldsymbol{X} - \mathcal{P}[\boldsymbol{X}]$, which gives the last equality in (3.14) for $\boldsymbol{X} = \boldsymbol{\alpha} \times \boldsymbol{V}_{\boldsymbol{\alpha}}$, and $\mathcal{P}[\boldsymbol{X}]$ is the compatible part of $\boldsymbol{X}$. The term $\mathcal{P}[\boldsymbol{\alpha} \times \boldsymbol{V}_{\boldsymbol{\alpha}}]$ is thus the compatible slip generated by dislocation motion; it enters the rate of $\boldsymbol{R}$ as the source in (3.10). Substituting (3.14) and (3.10) into (3.13), the generated terms cancel, and the induced admissible plastic-distortion rate is

$$\boldsymbol{\eta} := \dot{\boldsymbol{\beta}}_p = \boldsymbol{\alpha} \times \boldsymbol{V}_{\boldsymbol{\alpha}} - \nabla\left(\boldsymbol{R}\boldsymbol{V}_R\right). \tag{3.15}$$

Thus the admissible plastic-distortion rate is determined by the two transport velocities $(\boldsymbol{V}_{\boldsymbol{\alpha}}, \boldsymbol{V}_R)$. This is the rate-level tangent direction used in the constrained Onsager principle below.

Since the curl of a gradient vanishes, the transport law (3.7) determines $\dot{\boldsymbol{\beta}}_p$ only up to a gradient. The first term in (3.15), which includes the compatible slip generated by dislocation motion, is the plastic-distortion rate of Kosevich and Mura [Kos62, Mur63], for which this gradient is zero; the second term is the gradient given by the transport of $\boldsymbol{R}$. Physically, the former corresponds to plastic distortion evolution due to dislocation transport, and the latter corresponds to the plastic distortion evolution due to coherent interfacial motion of slip planes (if this occurs). We also refer to Sozio and Yavari [SY23] for an interesting discussion related to the fixing of the gauge.

---

much more likely it is accommodated by the compatible slip left behind by the motion of dislocations. To suppress the former deformation mechanism, we can set $\boldsymbol{V}_R \equiv \boldsymbol{0}$ or equivalently that the corresponding mobility coefficient vanishes.

4. Constrained Gradient Flow for Dislocation Evolution

An unconstrained gradient flow permits arbitrary rates of the plastic distortion $\boldsymbol{\beta}_p$. In contrast, the formulation developed here restricts the evolution to the transport-generated directions derived in Section 3. The transport velocities, rather than arbitrary rates of the state variables, are therefore the kinematic variables over which the variational principle is posed.

The guiding analogy is the Wasserstein formulation of dissipative evolution, in which admissible state rates are generated by transport velocities and the velocity is selected variationally through an Onsager principle [JKO98, AGS08, San15, Ons31, Doi11]. In the present setting, the ordinary continuity equation is replaced by the transport laws for $\boldsymbol{\alpha}$ and $\boldsymbol{R}$. The transport velocities therefore generate the admissible tangent directions and serve as the variational unknowns. We first derive the resulting transport-constrained Onsager evolution and subsequently identify its associated metric structure analogous to the Wasserstein Riemannian formulation.

4.A. Transport-Constrained Onsager Principle

We now apply Onsager's variational principle [Ons31, Doi11] to the transport-admissible velocities. The state variables are $(\boldsymbol{\alpha}, \boldsymbol{R})$, and the plastic distortion is reconstructed according to (2.2). Thus, $\boldsymbol{\beta}_p$ is not varied independently; its rate is induced by the admissible rates of $\boldsymbol{\alpha}$ and $\boldsymbol{R}$ following (3.15).

We begin by defining

$$s_{\boldsymbol{\alpha}} := \operatorname{curl}(\boldsymbol{\alpha} \times \boldsymbol{V}_{\boldsymbol{\alpha}}), \qquad (s_R)_{ij} := (\mathcal{P}[\boldsymbol{\alpha} \times \boldsymbol{V}_{\boldsymbol{\alpha}}])_{ij} - \partial_j \left(R_{ik} V_R^k\right) \tag{4.1}$$

as the transport-admissible rates generated by the velocities $(\boldsymbol{V}_{\boldsymbol{\alpha}}, \boldsymbol{V}_R)$. Then, the first variation of the reduced free energy along an admissible tangent direction $(s_{\boldsymbol{\alpha}}, s_R)$ is

$$D\mathcal{F}^{\mathrm{red}}[\boldsymbol{\alpha}, \boldsymbol{R}][s_{\boldsymbol{\alpha}}, s_R] = \int_\Omega \left[(-\boldsymbol{\sigma}^* + \boldsymbol{P}_\Psi) : \boldsymbol{\eta} + \boldsymbol{P}_\alpha^{\mathrm{d}} : s_{\boldsymbol{\alpha}} + \boldsymbol{P}_R^{\mathrm{d}} : \nabla s_R\right] \, \mathrm{d}\Omega. \tag{4.2}$$

For brevity, we define the effective thermodynamic stress-like quantity

$$\boldsymbol{\sigma}^{\mathrm{eff}} := \boldsymbol{\sigma}^* - \boldsymbol{P}_\Psi. \tag{4.3}$$

The Onsager functional is therefore

$$\mathcal{J}[\boldsymbol{V}_{\boldsymbol{\alpha}}, \boldsymbol{V}_R] := \frac{1}{2} \int_\Omega \boldsymbol{V}_{\boldsymbol{\alpha}} \cdot \boldsymbol{M}_{\boldsymbol{\alpha}}^{-1} \boldsymbol{V}_{\boldsymbol{\alpha}} \, \mathrm{d}\Omega + \frac{1}{2} \int_\Omega \boldsymbol{V}_R \cdot \boldsymbol{M}_R^{-1} \boldsymbol{V}_R \, \mathrm{d}\Omega + D\mathcal{F}^{\mathrm{red}}[\boldsymbol{\alpha}, \boldsymbol{R}][s_{\boldsymbol{\alpha}}, s_R], \tag{4.4}$$

with $s_{\boldsymbol{\alpha}}$ and s_R given by (4.1), and with $\boldsymbol{\eta}$ given by (3.15). The tensors $\boldsymbol{M}_{\boldsymbol{\alpha}}$ and $\boldsymbol{M}_R$ are the defect mobilities, which may depend on the state. We assume decoupled kinetics for simplicity. More general coupled kinetics can be described by a symmetric positive-definite mobility operator $\mathbb{M}$ acting on $\boldsymbol{V} = (\boldsymbol{V}_{\boldsymbol{\alpha}}, \boldsymbol{V}_R)$. This gives $\boldsymbol{V}^* = \mathbb{M}\boldsymbol{f}$, where $\boldsymbol{f} = (\boldsymbol{f}_{\boldsymbol{\alpha}}, \boldsymbol{f}_R)$, and preserves the energy-dissipation structure.

The transport velocities are selected by minimizing this functional:

$$(\boldsymbol{V}_{\boldsymbol{\alpha}}^*, \boldsymbol{V}_R^*) := \operatorname*{arg\,min}_{\boldsymbol{V}_{\boldsymbol{\alpha}}, \boldsymbol{V}_R} \mathcal{J}[\boldsymbol{V}_{\boldsymbol{\alpha}}, \boldsymbol{V}_R]. \tag{4.5}$$

The resulting evolution is then obtained by substituting the minimizing velocities into the transport equations:

$$\dot{\boldsymbol{\alpha}} = \operatorname{curl}(\boldsymbol{\alpha} \times \boldsymbol{V}_{\boldsymbol{\alpha}}^*), \qquad \dot{R}_{ij} = (\mathcal{P}[\boldsymbol{\alpha} \times \boldsymbol{V}_{\boldsymbol{\alpha}}^*])_{ij} - \partial_j \left(R_{ik} (V_R^*)^k\right). \tag{4.6}$$

Thus, Onsager's principle selects the transport velocities of the constrained gradient flow rather than the arbitrariness of the rate of the plastic distortion.

4.B. Driving Forces and Transport Closure

We first derive the thermodynamic driving forces associated with the dislocation density and the compatible slip. We then use these forces in the Onsager principle to obtain the transport closure.

4.B.1. Driving Force for the Evolution of the Dislocation Density

We denote the reduced elastic energy contribution by

$$E^{\mathrm{el}}[\boldsymbol{\alpha}, \boldsymbol{R}] := \int_\Omega W_e(\nabla \boldsymbol{u}^* - \boldsymbol{\beta}_p) \, \mathrm{d}\Omega - \int_{\partial\Omega_N} \bar{\boldsymbol{t}} \cdot \boldsymbol{u}^* \, \mathrm{d}\Gamma, \tag{4.7}$$

where $\boldsymbol{\beta}_p = \mathcal{C}[\boldsymbol{\alpha}] + \boldsymbol{R}$ and $\boldsymbol{u}^* = \boldsymbol{u}^*[\boldsymbol{\alpha}, \boldsymbol{R}]$ is the equilibrium displacement.

We likewise denote the lattice-energy contribution by

$$E^{\mathrm{lat}}[\boldsymbol{\alpha}, \boldsymbol{R}] := \int_\Omega \Psi(\boldsymbol{\beta}_p)\, \mathrm{d}\Omega. \tag{4.8}$$

We also denote the defect-energy contributions associated with $\boldsymbol{\alpha}$ and $\boldsymbol{R}$ by

$$E^{\alpha}[\boldsymbol{\alpha}] := \int_\Omega W_\alpha(\boldsymbol{\alpha})\, \mathrm{d}\Omega, \qquad E^{R}[\boldsymbol{R}] := \int_\Omega W_R(\nabla \boldsymbol{R})\, \mathrm{d}\Omega. \tag{4.9}$$

Because $\boldsymbol{u}^*$ satisfies elastic equilibrium, the variation of the reduced elastic energy contribution along an admissible plastic-distortion rate $\boldsymbol{\eta}$ is

$$\delta E^{\mathrm{el}} = -\int_\Omega \boldsymbol{\sigma}^* : \boldsymbol{\eta}\, \mathrm{d}\Omega. \tag{4.10}$$

The corresponding variation of the lattice energy is

$$\delta E^{\mathrm{lat}} = \int_\Omega \frac{\partial \Psi}{\partial \boldsymbol{\beta}_p} : \boldsymbol{\eta}\, \mathrm{d}\Omega. \tag{4.11}$$

Using $\boldsymbol{\sigma}^{\mathrm{eff}}$ defined in (4.3) and the induced plastic-distortion rate from (3.15), we have:

$$\delta E^{\mathrm{el}} + \delta E^{\mathrm{lat}} = -\int_\Omega \boldsymbol{\sigma}^{\mathrm{eff}} : (\boldsymbol{\alpha} \times \boldsymbol{V}_{\boldsymbol{\alpha}})\ \mathrm{d}\Omega + \int_\Omega \boldsymbol{\sigma}^{\mathrm{eff}} : \nabla\left(\boldsymbol{R}\boldsymbol{V}_R\right)\ \mathrm{d}\Omega. \tag{4.12}$$

The defect-energy variation associated with $\boldsymbol{\alpha}$ is

$$\delta E^{\alpha} = \int_\Omega \boldsymbol{P}^{\mathrm{d}}_{\alpha} : \mathrm{curl}\left(\boldsymbol{\alpha} \times \boldsymbol{V}_{\boldsymbol{\alpha}}\right)\ \mathrm{d}\Omega, \tag{4.13}$$

where we have used $\boldsymbol{P}^{\mathrm{d}}_{\alpha}$ defined in (2.12). After integrating by parts under the boundary conditions of Section 2.B.1, this can be written as

$$\delta E^{\alpha} = \int_\Omega \boldsymbol{V}_{\boldsymbol{\alpha}} \cdot \sum_i \left[\left(\mathrm{curl}\, \boldsymbol{P}^{\mathrm{d}}_{\alpha,i}\right) \times \boldsymbol{\alpha}_i\right]\ \mathrm{d}\Omega. \tag{4.14}$$

Combining all of the variational terms gives the $\boldsymbol{\alpha}$-driving force; the term involving $\boldsymbol{P}^{\mathrm{d}}_R$ arises from W_R through the compatible slip generated by dislocation motion, and is derived after (4.23):

$$\boldsymbol{f}_{\boldsymbol{\alpha}} = \sum_i \left[\left(\boldsymbol{\sigma}^{\mathrm{eff}}_i - \mathrm{curl}\, \boldsymbol{P}^{\mathrm{d}}_{\alpha,i} + \left(\mathcal{P}[\mathrm{div}\, \boldsymbol{P}^{\mathrm{d}}_R]\right)_i\right) \times \boldsymbol{\alpha}_i\right]. \tag{4.15}$$

4.B.2. Driving Force for the Evolution of the Compatible Slip

For the compatible slip, we first consider the part of the admissible tangent direction generated by $\boldsymbol{V}_R$; the part generated by dislocation motion is treated after (4.23):

$$(s_R)_{ij} = -\partial_j \left(R_{ik} V^k_R\right). \tag{4.16}$$

The combined elastic and lattice-energy contribution associated with this tangent direction is

$$-\int_\Omega \boldsymbol{\sigma}^{\mathrm{eff}} : s_R\, \mathrm{d}\Omega = \int_\Omega \sigma^{\mathrm{eff}}_{ij} \partial_j \left(R_{ik} V^k_R\right)\ \mathrm{d}\Omega. \tag{4.17}$$

The compatible slip energy contribution is

$$\delta E^{R} = \int_\Omega \boldsymbol{P}^{\mathrm{d}}_R : \nabla s_R\, \mathrm{d}\Omega, \tag{4.18}$$

where we use $\boldsymbol{P}_R^{\mathrm{d}}$ defined in (2.12). After integrating by parts under the boundary conditions of Section 2.B.1,

$$\delta E^R = -\int_\Omega \operatorname{div} \boldsymbol{P}_R^{\mathrm{d}} : s_R \,\mathrm{d}\Omega = \int_\Omega \left(\operatorname{div} \boldsymbol{P}_R^{\mathrm{d}}\right)_{ij} \partial_j \left(R_{ik} V_R^k\right) \,\mathrm{d}\Omega. \tag{4.19}$$

Therefore, the combined contribution associated with the compatible slip is

$$\int_\Omega \left(\boldsymbol{\sigma}^{\mathrm{eff}} + \operatorname{div} \boldsymbol{P}_R^{\mathrm{d}}\right)_{ij} \partial_j \left(R_{ik} V_R^k\right) \,\mathrm{d}\Omega = -\int_\Omega \partial_j \left(\boldsymbol{\sigma}^{\mathrm{eff}} + \operatorname{div} \boldsymbol{P}_R^{\mathrm{d}}\right)_{ij} R_{ik} V_R^k \,\mathrm{d}\Omega. \tag{4.20}$$

This can be written as

$$-\int_\Omega \boldsymbol{V}_R \cdot \boldsymbol{f}_R \,\mathrm{d}\Omega, \tag{4.21}$$

where

$$(\boldsymbol{f}_R)_k = R_{ik} \partial_j \left(\boldsymbol{\sigma}^{\mathrm{eff}} + \operatorname{div} \boldsymbol{P}_R^{\mathrm{d}}\right)_{ij}. \tag{4.22}$$

Here, $\boldsymbol{\sigma}_i^{\mathrm{eff}}$, $\boldsymbol{P}_{\alpha,i}^{\mathrm{d}}$, and $\boldsymbol{\alpha}_i$ denote the i-th rows of the corresponding tensor fields, and repeated indices are summed. In addition,

$$\left(\operatorname{div} \boldsymbol{P}_R^{\mathrm{d}}\right)_{ij} := \partial_k \left(\boldsymbol{P}_R^{\mathrm{d}}\right)_{ijk}. \tag{4.23}$$

The part $\mathcal{P}[\boldsymbol{\alpha} \times \boldsymbol{V}_{\boldsymbol{\alpha}}]$ of s_R generated by dislocation motion does not change $\boldsymbol{\eta}$ and enters only through W_R. Integrating by parts as in (4.19), and using that, by (3.12), $\mathcal{P}$ is the L^2-orthogonal projection onto gradient fields, its contribution is

$$\int_\Omega \boldsymbol{P}_R^{\mathrm{d}} : \nabla \mathcal{P}[\boldsymbol{\alpha} \times \boldsymbol{V}_{\boldsymbol{\alpha}}] \,\mathrm{d}\Omega = -\int_\Omega \mathcal{P}[\operatorname{div} \boldsymbol{P}_R^{\mathrm{d}}] : (\boldsymbol{\alpha} \times \boldsymbol{V}_{\boldsymbol{\alpha}}) \,\mathrm{d}\Omega = -\int_\Omega \boldsymbol{V}_{\boldsymbol{\alpha}} \cdot \sum_i \left(\mathcal{P}[\operatorname{div} \boldsymbol{P}_R^{\mathrm{d}}]\right)_i \times \boldsymbol{\alpha}_i \,\mathrm{d}\Omega, \tag{4.24}$$

which gives the last term in (4.15). This term vanishes for $W_R = 0$, as in Sections 5–7.

4.B.3. Transport Closure from the Onsager Principle

The driving forces in (4.15) and (4.22) have related precedents in the literature. The former has the generalized Peach–Koehler structure found in continuum dislocation mechanics [Mur13], with the defect-energy contribution having the same overall physical origina as the energetic back-stresses [Gur04, Hoc16], while its lattice-energy contribution is related to Peierls-type models [KCO02]. Since $\boldsymbol{R} = \nabla \boldsymbol{A}$, the transport part of its evolution corresponds to advection of $\boldsymbol{A}$, up to an additive time-dependent constant. Viewing $\mathcal{F}^{\mathrm{red}}[\boldsymbol{\alpha}, \nabla \boldsymbol{A}]$ as a functional of $\boldsymbol{A}$ at fixed $\boldsymbol{\alpha}$, with variations of $\boldsymbol{A}$ that vanish near $\partial\Omega$, we can write (4.22) as

$$(\boldsymbol{f}_R)_k = R_{ik} \frac{\delta \mathcal{F}^{\mathrm{red}}}{\delta A_i}, \qquad \frac{\delta \mathcal{F}^{\mathrm{red}}}{\delta A_i} = \partial_j \left(\boldsymbol{\sigma}^{\mathrm{eff}} + \operatorname{div} \boldsymbol{P}_R^{\mathrm{d}}\right)_{ij}. \tag{4.25}$$

The transport of the compatible gradient field is kinematically analogous to interface-density transport in Agrawal and Dayal [AD15a]. However, their interface kinetics are prescribed constitutively, whereas here the transport velocity is selected through the constrained Onsager principle. Since (3.10) makes (3.15) exact, both driving forces are obtained from the exact reduced-energy variation along the transport-admissible rates.

Combining all energetic contributions under the boundary conditions of Section 2.B.1, the reduced-energy variation can be written as

$$\delta \mathcal{F}^{\mathrm{red}} = -\int_\Omega \boldsymbol{V}_{\boldsymbol{\alpha}} \cdot \boldsymbol{f}_{\boldsymbol{\alpha}} \,\mathrm{d}\Omega - \int_\Omega \boldsymbol{V}_R \cdot \boldsymbol{f}_R \,\mathrm{d}\Omega. \tag{4.26}$$

Substitution into (4.4) gives

$$\mathcal{J} = \frac{1}{2} \int_\Omega \boldsymbol{V}_{\boldsymbol{\alpha}} \cdot \boldsymbol{M}_{\boldsymbol{\alpha}}^{-1} \boldsymbol{V}_{\boldsymbol{\alpha}} \,\mathrm{d}\Omega + \frac{1}{2} \int_\Omega \boldsymbol{V}_R \cdot \boldsymbol{M}_R^{-1} \boldsymbol{V}_R \,\mathrm{d}\Omega - \int_\Omega \boldsymbol{V}_{\boldsymbol{\alpha}} \cdot \boldsymbol{f}_{\boldsymbol{\alpha}} \,\mathrm{d}\Omega - \int_\Omega \boldsymbol{V}_R \cdot \boldsymbol{f}_R \,\mathrm{d}\Omega. \tag{4.27}$$

Stationarity with respect to the two transport velocities yields

$$\boldsymbol{V}_{\boldsymbol{\alpha}}^* = \boldsymbol{M}_{\boldsymbol{\alpha}} \boldsymbol{f}_{\boldsymbol{\alpha}}, \qquad \boldsymbol{V}_R^* = \boldsymbol{M}_R \boldsymbol{f}_R. \tag{4.28}$$

Substituting the optimal velocities into the transport laws gives the transport-constrained evolution system

$$\dot{\boldsymbol{\alpha}} = \operatorname{curl}\left(\boldsymbol{\alpha} \times \boldsymbol{M}_{\boldsymbol{\alpha}} \boldsymbol{f}_{\boldsymbol{\alpha}}\right), \tag{4.29a}$$

$$\dot{R}_{ij} = \left(\mathcal{P}[\boldsymbol{\alpha} \times \boldsymbol{M}_{\boldsymbol{\alpha}} \boldsymbol{f}_{\boldsymbol{\alpha}}]\right)_{ij} - \partial_j \left[R_{ik} \left(\boldsymbol{M}_R \boldsymbol{f}_R\right)^k\right]. \tag{4.29b}$$

This system is the transport-constrained evolution generated by the Onsager principle. Its corresponding metric and gradient-flow interpretation, analogous to the Riemannian formulation, are developed in Section 4.C.

4.C. Transport Manifold, Dissipation Metric, and Gradient-Flow Structure

Having derived the transport-constrained Onsager evolution and its driving forces, we now identify the associated geometric structure. The construction below should be understood as a formal interpretation of the resulting evolution rather than as a necessary element in its derivation.

Motivated by the formal Riemannian interpretation of Wasserstein gradient flows [Ott01], we define a state-dependent transport metric for the variables $(\boldsymbol{\alpha}, \boldsymbol{R})$. The role played by the continuity equation in the Wasserstein setting is played here by the transport laws for $\boldsymbol{\alpha}$ and the compatible slip $\boldsymbol{R}$. The metric is therefore not imposed directly on arbitrary rates of the state variables, but is defined through the minimum dissipation of velocity fields that generate a prescribed admissible tangent direction.

The state space is the transport manifold

$$\mathcal{M} := \{(\boldsymbol{\alpha}, \boldsymbol{R}) : \operatorname{div} \boldsymbol{\alpha} = \boldsymbol{0}, \qquad \operatorname{curl} \boldsymbol{R} = \boldsymbol{0}, \qquad \boldsymbol{\beta}_p = \mathcal{C}[\boldsymbol{\alpha}] + \boldsymbol{R}\}. \tag{4.30}$$

We work formally on the bounded, smooth, simply connected domain Ω with connected boundary, using the decomposition and boundary conditions specified in Section 2.B. We take $\boldsymbol{\alpha}, \boldsymbol{R} \in L^2(\Omega)$, with $\boldsymbol{R} \in H^1(\Omega)$ when $W_R \neq 0$, and impose the divergence and curl constraints in the distributional sense. The derivations assume sufficiently smooth fields, finite energy, and transport velocities of finite dissipation. The boundary terms in the integrations by parts vanish under the conditions of Section 2.B.1. Although the compatibility constraints defining $\mathcal{M}$ are linear, the transport-generated directions generally do not span its full tangent space. Consequently, the evolution is restricted to states reachable from the initial state by transport.

At a state $(\boldsymbol{\alpha}, \boldsymbol{R}) \in \mathcal{M}$, we denote by $T^{\mathrm{tr}}_{(\boldsymbol{\alpha},\boldsymbol{R})}\mathcal{M}$ the transport-admissible tangent space to $\mathcal{M}$ at $(\boldsymbol{\alpha}, \boldsymbol{R})$, where T denotes the tangent space and the superscript tr indicates restriction to transport-generated directions. It is defined by

$$T^{\mathrm{tr}}_{(\boldsymbol{\alpha},\boldsymbol{R})}\mathcal{M} := \left\{ (s_{\boldsymbol{\alpha}}, s_R) : \begin{array}{l} s_{\boldsymbol{\alpha}} = \operatorname{curl}\left(\boldsymbol{\alpha} \times \boldsymbol{V}_{\boldsymbol{\alpha}}\right), \\ (s_R)_{ij} = \left(\mathcal{P}[\boldsymbol{\alpha} \times \boldsymbol{V}_{\boldsymbol{\alpha}}]\right)_{ij} - \partial_j \left(R_{ik} V_R^k\right) \end{array} \text{ for some } (\boldsymbol{V}_{\boldsymbol{\alpha}}, \boldsymbol{V}_R) \right\}. \tag{4.31}$$

Here, $\boldsymbol{V}_{\boldsymbol{\alpha}}$ is the transport velocity associated with the evolution of the dislocation density tensor governed by the dislocation transport law, while $\boldsymbol{V}_R$ is the transport velocity associated with the compatible slip $\boldsymbol{R}$. Thus $s_{\boldsymbol{\alpha}}$ and s_R are not arbitrary variations; they are precisely the tangent directions generated by the admissible transport velocities.

Each admissible tangent direction $(s_{\boldsymbol{\alpha}}, s_R)$ induces the plastic-distortion rate $\boldsymbol{\eta}$ given in (3.15). Thus, $\boldsymbol{\eta}$ is not an independent tangent direction on $\mathcal{M}$, but is induced by the admissible transport velocities associated with $(s_{\boldsymbol{\alpha}}, s_R)$. We assume that the mobility tensors $\boldsymbol{M}_{\boldsymbol{\alpha}}$ and $\boldsymbol{M}_R$ are symmetric positive definite. We define the corresponding transport metric by assigning a kinetic cost to the transport velocities. For an admissible tangent direction $(s_{\boldsymbol{\alpha}}, s_R)$, set

$$g_{(\boldsymbol{\alpha},\boldsymbol{R})}\left((s_{\boldsymbol{\alpha}}, s_R), (s_{\boldsymbol{\alpha}}, s_R)\right) := \inf \int_\Omega \left[\boldsymbol{V}_{\boldsymbol{\alpha}} \cdot \boldsymbol{M}_{\boldsymbol{\alpha}}^{-1} \boldsymbol{V}_{\boldsymbol{\alpha}} + \boldsymbol{V}_R \cdot \boldsymbol{M}_R^{-1} \boldsymbol{V}_R\right] \mathrm{d}\Omega. \tag{4.32}$$

The infimum is taken over all velocity fields $(\boldsymbol{V}_{\boldsymbol{\alpha}}, \boldsymbol{V}_R)$ satisfying

$$s_{\boldsymbol{\alpha}} = \operatorname{curl}\left(\boldsymbol{\alpha} \times \boldsymbol{V}_{\boldsymbol{\alpha}}\right), \qquad (s_R)_{ij} = \left(\mathcal{P}[\boldsymbol{\alpha} \times \boldsymbol{V}_{\boldsymbol{\alpha}}]\right)_{ij} - \partial_j \left(R_{ik} V_R^k\right). \tag{4.33}$$

Equivalently, the metric measures the least dissipation required to realize a given admissible tangent direction. This is the direct analog of the Wasserstein metric, where a density tangent direction is measured by the least kinetic energy of a velocity field producing it through the continuity equation. Here the admissible tangent directions are generated instead by the transport law for $\boldsymbol{\alpha}$ and by the evolution law (3.10) for the compatible slip $\boldsymbol{R}$.

We now make precise the sense in which the constrained Onsager evolution can be interpreted as a gradient flow of the reduced free energy $\mathcal{F}^{\mathrm{red}}$ with respect to the transport metric (4.32). The following result is formal and is intended in the formal Riemannian sense described above: admissible tangent directions are generated by transport velocities, and the metric assigns to each tangent direction the minimum dissipation among the velocity fields that realize it. Equivalently, velocity fields that generate the same tangent direction are identified through their minimum-dissipation representative.

Throughout this subsection, we assume sufficient regularity of the state and velocity fields, and the existence of the required minimum-dissipation representatives. The rigorous proof by Otto for mass transport in porous media [Ott01] uses special

properties of the scalar Wasserstein/porous-medium problem, including approximation and compactness results that we have not established for our transport system governed by the dislocation transport law. Our transport map is more complicated and has a nontrivial kernel, so we would need results for the induced metric, weak solutions, and convergence. Consequently, a complete metric-space theory, including the rigorous construction of the induced transport distance and a corresponding weak-solution framework, is beyond the scope of the present work.

The integrations by parts are understood under the boundary conditions of Section 2.B.1.

Proposition 4.1 (Formal gradient-flow identity)**.** *Let $(\boldsymbol{\alpha}(t), \boldsymbol{R}(t)) \in \mathcal{M}$ be a smooth solution of the transport-constrained evolution system* (4.29)*, where the driving forces $\boldsymbol{f}_{\boldsymbol{\alpha}}$ and $\boldsymbol{f}_R$ are defined by* (4.15) *and* (4.22)*. Assume that the mobility tensors $\boldsymbol{M}_{\boldsymbol{\alpha}}$ and $\boldsymbol{M}_R$ are symmetric positive definite.*

Then, for every admissible tangent direction

$$(s_{\boldsymbol{\alpha}}, s_R) \in T^{\mathrm{tr}}_{(\boldsymbol{\alpha},\boldsymbol{R})}\mathcal{M}, \tag{4.34}$$

the constrained evolution satisfies

$$g_{(\boldsymbol{\alpha},\boldsymbol{R})}\left((\dot{\boldsymbol{\alpha}}, \dot{\boldsymbol{R}}), (s_{\boldsymbol{\alpha}}, s_R)\right) + D\mathcal{F}^{\mathrm{red}}(\boldsymbol{\alpha}, \boldsymbol{R})[s_{\boldsymbol{\alpha}}, s_R] = 0. \tag{4.35}$$

Consequently, for time-independent external loading,

$$\frac{\mathrm{d}}{\mathrm{d}t}\mathcal{F}^{\mathrm{red}}[\boldsymbol{\alpha}, \boldsymbol{R}] = -\int_\Omega \boldsymbol{f}_{\boldsymbol{\alpha}} \cdot \boldsymbol{M}_{\boldsymbol{\alpha}} \boldsymbol{f}_{\boldsymbol{\alpha}} \,\mathrm{d}\Omega - \int_\Omega \boldsymbol{f}_R \cdot \boldsymbol{M}_R \boldsymbol{f}_R \,\mathrm{d}\Omega \le 0. \tag{4.36}$$

Thus, in the formal Riemannian sense induced by the transport metric,

$$(\dot{\boldsymbol{\alpha}}, \dot{\boldsymbol{R}}) = -\operatorname{grad}_g \mathcal{F}^{\mathrm{red}}(\boldsymbol{\alpha}, \boldsymbol{R}). \tag{4.37}$$

Proof. Let

$$(s_{\boldsymbol{\alpha}}, s_R) \in T^{\mathrm{tr}}_{(\boldsymbol{\alpha},\boldsymbol{R})}\mathcal{M} \tag{4.38}$$

be an arbitrary admissible tangent direction. By definition, there exist test transport velocities $(\boldsymbol{W}_{\boldsymbol{\alpha}}, \boldsymbol{W}_R)$ such that

$$s_{\boldsymbol{\alpha}} = \operatorname{curl}(\boldsymbol{\alpha} \times \boldsymbol{W}_{\boldsymbol{\alpha}}), \qquad (s_R)_{ij} = (\mathcal{P}[\boldsymbol{\alpha} \times \boldsymbol{W}_{\boldsymbol{\alpha}}])_{ij} - \partial_j\left(R_{ik} W_R^k\right). \tag{4.39}$$

Here, s_R is the tangent direction for the compatible slip $\boldsymbol{R}$. Since $\boldsymbol{R}$ itself enters the reconstruction $\boldsymbol{\beta}_p = \mathcal{C}[\boldsymbol{\alpha}] + \boldsymbol{R}$, no additional kinematic tangent direction ∇s_R is introduced. Gradients of s_R enter only through the variation of the regularizing energy $W_R(\nabla \boldsymbol{R})$, when such an energy is included. When several velocity fields generate the same tangent direction, we take $(\boldsymbol{W}_{\boldsymbol{\alpha}}, \boldsymbol{W}_R)$ to be the minimum-dissipation representative appearing in the definition of the metric (4.32). With this convention, the metric pairing is independent of the representative.

Using the force representation of the reduced-energy variation, the directional derivative of $\mathcal{F}^{\mathrm{red}}$ along $(s_{\boldsymbol{\alpha}}, s_R)$ is

$$D\mathcal{F}^{\mathrm{red}}(\boldsymbol{\alpha}, \boldsymbol{R})[s_{\boldsymbol{\alpha}}, s_R] = -\int_\Omega \boldsymbol{W}_{\boldsymbol{\alpha}} \cdot \boldsymbol{f}_{\boldsymbol{\alpha}} \,\mathrm{d}\Omega - \int_\Omega \boldsymbol{W}_R \cdot \boldsymbol{f}_R \,\mathrm{d}\Omega. \tag{4.40}$$

The lattice energy contribution is included in this force representation through the effective thermodynamic stress $\boldsymbol{\sigma}^{\mathrm{eff}}$ defined in (4.3), which enters both $\boldsymbol{f}_{\boldsymbol{\alpha}}$ and $\boldsymbol{f}_R$.

On the other hand, the constrained Onsager principle gives the optimal velocities in (4.28). Substitution of these velocities into the transport laws gives the actual tangent direction in (4.6).

Using the bilinear form induced by the transport metric and the minimum-dissipation velocity representatives, we obtain

$$g_{(\boldsymbol{\alpha},\boldsymbol{R})}\left((\dot{\boldsymbol{\alpha}}, \dot{\boldsymbol{R}}), (s_{\boldsymbol{\alpha}}, s_R)\right) + D\mathcal{F}^{\mathrm{red}}(\boldsymbol{\alpha}, \boldsymbol{R})\,[s_{\boldsymbol{\alpha}}, s_R] = \int_\Omega \boldsymbol{W}_{\boldsymbol{\alpha}} \cdot \left(\boldsymbol{M}_{\boldsymbol{\alpha}}^{-1} \boldsymbol{V}_{\boldsymbol{\alpha}}^* - \boldsymbol{f}_{\boldsymbol{\alpha}}\right) \mathrm{d}\Omega + \int_\Omega \boldsymbol{W}_R \cdot \left(\boldsymbol{M}_R^{-1} \boldsymbol{V}_R^* - \boldsymbol{f}_R\right) \mathrm{d}\Omega. \tag{4.41}$$

By (4.28), the right-hand side vanishes.

$$g_{(\boldsymbol{\alpha},\boldsymbol{R})}\left((\dot{\boldsymbol{\alpha}}, \dot{\boldsymbol{R}}), (s_{\boldsymbol{\alpha}}, s_R)\right) + D\mathcal{F}^{\mathrm{red}}(\boldsymbol{\alpha}, \boldsymbol{R})[s_{\boldsymbol{\alpha}}, s_R] = 0. \tag{4.42}$$

This proves (4.35).

It remains to derive the energy-dissipation identity. Along smooth solutions and for time-independent prescribed loads, the chain rule gives

$$\frac{\mathrm{d}}{\mathrm{d}t}\mathcal{F}^{\mathrm{red}}[\boldsymbol{\alpha},\boldsymbol{R}] = D\mathcal{F}^{\mathrm{red}}(\boldsymbol{\alpha},\boldsymbol{R})[\dot{\boldsymbol{\alpha}},\dot{\boldsymbol{R}}]. \tag{4.43}$$

Taking

$$(s_{\boldsymbol{\alpha}}, s_R) = (\dot{\boldsymbol{\alpha}},\dot{\boldsymbol{R}}) \tag{4.44}$$

in (4.35), we obtain

$$\frac{\mathrm{d}}{\mathrm{d}t}\mathcal{F}^{\mathrm{red}}[\boldsymbol{\alpha},\boldsymbol{R}] = -g_{(\boldsymbol{\alpha},\boldsymbol{R})}\left((\dot{\boldsymbol{\alpha}},\dot{\boldsymbol{R}}),(\dot{\boldsymbol{\alpha}},\dot{\boldsymbol{R}})\right). \tag{4.45}$$

Using the optimal velocities (4.28) gives precisely the energy-dissipation identity (4.36). □

The proposition shows that the constrained Onsager system is a gradient flow with respect to the transport metric on the state variables $(\boldsymbol{\alpha},\boldsymbol{R})$. The role of the metric is to measure the least dissipation required to generate an admissible tangent direction through the transport velocities. Thus, the velocity fields are the variables selected by the Onsager principle, while the state rates $(\dot{\boldsymbol{\alpha}},\dot{\boldsymbol{R}})$ are induced by the transport laws.

5. Dislocation Driving Force and Reduction to the Classical Peach–Koehler Limit

The dislocation driving force in (4.15) differs from the classical Peach–Koehler force on a dislocation; the elastic terms correspond to the classical expression, but the defect energy and the lattice energy provide – as expected – additional contributions. Importantly, these contributions are not appended independently to the transport law but instead follow from the variation of the energy along transport-admissible directions.

The defect energy contribution to the dislocation driving force is:

$$\boldsymbol{f}_{\boldsymbol{\alpha}}^{\mathrm{def}} = \sum_i \left[-\operatorname{curl}\boldsymbol{P}_{\alpha,i}^{\mathrm{d}}\right]\times\boldsymbol{\alpha}_i. \tag{5.1}$$

Related defect-energy, back-stress, line-tension, gradient, and curvature contributions arise in continuum dislocation theories [GCZ03, Zai15, Hoc16, Cla15].

To consider the lattice energy contribution, we first neglect the defect and compatible slip regularizing energies, i.e., $W_\alpha = W_R = 0$. The driving forces for $\boldsymbol{\alpha}$ and $\boldsymbol{R}$ reduce to:

$$\boldsymbol{f}_{\boldsymbol{\alpha}} = \sum_i \boldsymbol{\sigma}_i^{\mathrm{eff}}\times\boldsymbol{\alpha}_i. \tag{5.2a}$$

$$(\boldsymbol{f}_R)_k = R_{ik}\partial_j\boldsymbol{\sigma}_{ij}^{\mathrm{eff}}. \tag{5.2b}$$

Consequently, when the defect and compatible slip regularizing energies are neglected, the constrained Onsager principle yields a generalized Peach–Koehler-type transport force. This generalized Peach–Koehler force has the same structure as the classical Peach–Koehler force, but with the effective thermodynamic stress $\boldsymbol{\sigma}^{\mathrm{eff}}$ replacing the standard elastic stress. The compatible slip $\boldsymbol{R}$ is driven by its coupling to the effective thermodynamic stress through the reconstructed plastic distortion.

Remark 5.1 (Recovery of the Classical Peach–Koehler Force for a Single Dislocation Line)**.** We show that the generalized dislocation driving force reduces to the classical Peach–Koehler force for a single dislocation line. Consider a dislocation with Burgers vector $\boldsymbol{b}$ and line direction $\boldsymbol{\xi}$. Its dislocation density tensor is

$$\boldsymbol{\alpha} = \boldsymbol{b}\otimes\boldsymbol{\xi}\,\delta_L, \tag{5.3}$$

where δ_L denotes concentration on the dislocation line L. Thus, row-wise,

$$\boldsymbol{\alpha}_i = b_i\boldsymbol{\xi}\,\delta_L. \tag{5.4}$$

Substitution into (5.2a) gives the force per unit length

$$\boldsymbol{f}_{\mathrm{line}}^{\mathrm{eff}} = \sum_i b_i\left(\boldsymbol{\sigma}_i^{\mathrm{eff}}\times\boldsymbol{\xi}\right) = \left[\left(\boldsymbol{\sigma}^{\mathrm{eff}}\right)^T\boldsymbol{b}\right]\times\boldsymbol{\xi}. \tag{5.5}$$

This is a generalized Peach–Koehler-type force in which the lattice energy contributes to the elastic part. We highlight that, in general, $\boldsymbol{\sigma}^{\mathrm{eff}}$ may not be symmetric because $\dfrac{\partial \Psi}{\partial \boldsymbol{\beta}_p}$ may not be symmetric; therefore, the transpose in (5.5) cannot generally be omitted.

If we further neglect the lattice-energy contribution, i.e., $\dfrac{\partial \Psi}{\partial \boldsymbol{\beta}_p} = \mathbf{0}$, then $\boldsymbol{\sigma}^{\mathrm{eff}} = \boldsymbol{\sigma}^*$, and we recover the classical expression for the Peach–Koehler force on a dislocation line:

$$\boldsymbol{f}_{\mathrm{line}} = (\boldsymbol{\sigma}^* \boldsymbol{b}) \times \boldsymbol{\xi}, \tag{5.6}$$

where we can now use the symmetry of the stress tensor. See, for example, Ref. [KOPF20] for a modern discussion of driving forces on dislocations. □

6. Comparison with Cahn–Hilliard-type Phase Field Evolution

Phase-field and mesoscale formulations provide another important class of continuum descriptions of dislocation microstructure. Approaches developed by Koslowski, LeSar, and Thomson [KLT04], LeSar [LeS14], and Beyerlein and Hunter [BH16] illustrate how dislocation microstructure, plastic response, and defect interactions can be represented across scales. Such models motivate comparison with the present formulation, while also emphasizing that the choice of order parameter, conservation law, and admissible kinetics is central to the resulting evolution.

Within this broader class, Cahn–Hilliard dynamics provides a particularly useful comparison because it is a gradient flow with a conserved quantity [CH58, Cah61], and can also be expressed through a flux-based Rayleigh principle. The essential distinction lies in the underlying conservation law and admissible current: the relevant kinematics here are generated by the dislocation transport law rather than by the standard continuity equation as in the Cahn–Hilliard model.

For a conserved scalar order parameter q, the evolution may be written as

$$\dot{q} + \operatorname{div} \boldsymbol{J} = 0, \qquad \boldsymbol{J} = -M \nabla \mu, \qquad \mu = \frac{\delta \mathcal{F}}{\delta q} \implies \dot{q} = \operatorname{div}\left(M \nabla \mu\right), \tag{6.1}$$

where $\boldsymbol{J}$ is the flux, M is the mobility, and μ is the chemical potential which is the variational derivative of the free energy $\mathcal{F}$ with respect to q. This equation expresses the conservation of q through an ordinary diffusive flux driven by gradients of the chemical potential. For constant mobility, it is the H^{-1} gradient flow of the free energy; more general mobilities use the corresponding weighted H^{-1}-type structures [CTC97].

The same evolution can also be derived using an Onsager functional. Using $\dot{q} = -\operatorname{div} \boldsymbol{J}$, the free-energy rate is

$$\frac{\mathrm{d}}{\mathrm{d}t}\mathcal{F}[q] = \int_\Omega \mu\, \dot{q}\, \mathrm{d}\Omega = \int_\Omega \nabla \mu \cdot \boldsymbol{J}\, \mathrm{d}\Omega, \tag{6.2}$$

where the boundary term vanishes by the no-flux condition of Section 2.B.1. Minimizing the Rayleighian

$$\mathcal{R}_{\mathrm{CH}}[\boldsymbol{J}] := \frac{1}{2}\int_\Omega \boldsymbol{J} \cdot M^{-1} \boldsymbol{J}\, \mathrm{d}\Omega + \int_\Omega \nabla \mu \cdot \boldsymbol{J}\, \mathrm{d}\Omega \tag{6.3}$$

with respect to the flux gives $\boldsymbol{J} = -M \nabla \mu$ and hence recovers (6.1). Thus, the essential Cahn–Hilliard procedure consists of combining the appropriate conservation law with a free energy and a dissipation potential for the corresponding flux.

The corresponding conservation law for the dislocation density tensor is (3.7). Recalling the dislocation flux introduced in Section 3.A, we have:

$$\boldsymbol{J}_\alpha := \boldsymbol{\alpha} \times \boldsymbol{V}_\alpha \tag{6.4}$$

The requirement that the flux has the geometric structure above is a key distinction compared to the Cahn–Hilliard flux in (6.1). Consequently, the resulting negative-order metric for dislocation evolution is not a fixed H^{-1} norm as in the case of Cahn–Hilliard evolution. Because the transport operator associated with the dislocation transport law $\operatorname{curl}(\boldsymbol{\alpha} \times \boldsymbol{V}_\alpha)$ depends explicitly on the current dislocation density, the corresponding metric is state-dependent and is precisely the transport metric introduced in Section 4.C.

The Onsager functional approach can similarly be adapted by replacing the standard flux with the dislocation flux that is compatible with the dislocation transport law, and minimizing over the dislocation velocity (Section 4).

Recent phase-field interpretations of continuum dislocation dynamics have likewise emphasized that dislocation-density variables obey nonstandard conservation laws and that their evolution equations generally go beyond the classical distinction between Allen–Cahn and Cahn–Hilliard dynamics [ZWZ25]. For curved dislocations, the evolution of line density may contain transport, orientation, and curvature contributions, and the total line length need not be conserved.

7. Application to Dislocation Annihilation

We now specialize the general formulation to the evolution of two dislocations with equal and opposite Burgers charge, and study their annihilation dynamics. Our aim is to understand how the elastic, defect, nonconvex lattice, and applied stress contributions modify the dislocation interactions and dynamics.

We restrict the continuum fields to a single glide layer, on which they are described by a signed density $q(x_1, t)$. The transport law and the Onsager principle then give an evolution equation for q, which we solve numerically from Gaussian initial cores. We focus on narrow cores, for which the lattice energy is large compared with the elastic interaction at the core scale, as near closely spaced dislocation cores [HSRC20]. The cores then keep the Peierls–Nabarro width and glide toward annihilation, and a uniform resolved shear stress either assists annihilation or, above a threshold, separates the pair.

The calculations are illustrative rather than quantitative predictions for a specific material: the parameters have not been calibrated to a particular crystal, although first-principles calculations provide a route to such calibration [BS25].

7.A. Geometry and Modeling Assumptions

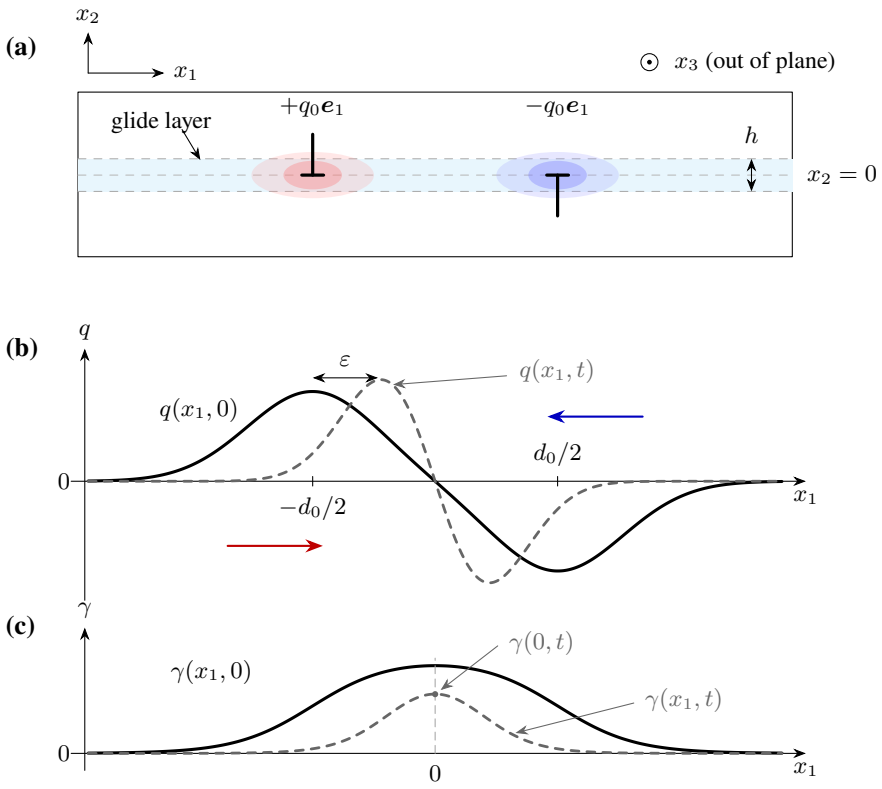


Figure 2. Schematic of the opposite-sign edge-dislocation pair. (a) The dislocations have Burgers vectors $\pm q_0\boldsymbol{e}_1$ and line direction $\boldsymbol{e}_3$, on a thin glide layer of thickness h centered at $x_2 = 0$. (b) Signed density q: initial state with two Gaussian cores of standard deviation ε centered at $x_1 = \mp d_0/2$ (solid), and a later state (dashed). The velocity reverses direction with the sign of q; when the net stress drives the cores together, positive and negative Burgers content move toward $x_1 = 0$ (arrows) and cancel there. (c) Slip γ, with $q = \partial_{x_1}\gamma$; the slip $\gamma(0, t)$ equals the Burgers content on either side of $x_1 = 0$ and decreases as the pair annihilates. All dimensions and profiles are schematic.

We consider two straight, parallel edge dislocations with Burgers vectors $\pm q_0\boldsymbol{e}_1$, $q_0 > 0$, line direction $\boldsymbol{e}_3$, and common glide plane $x_2 = 0$. The body is large compared with the initial separation d_0 and the core width, so that boundary and image effects are neglected, integrals along x_1 are taken over $\mathbb{R}$, and all energies are per unit dislocation-line length. Figure 2 illustrates the geometry and the evolution of the density. We make the following assumptions:

(i) Glide-layer kinematics: Slip is confined to a single glide layer $|x_2| < h/2$ of interplanar thickness h. The dislocation density and the compatible slip are

$$\begin{aligned} \boldsymbol{\alpha}(\boldsymbol{x}, t) &= \frac{q(x_1, t)}{h}\, \chi_h(x_2)\, \boldsymbol{e}_1 \otimes \boldsymbol{e}_3, \\ \boldsymbol{R}(\boldsymbol{x}, t) &= \frac{\gamma(x_1, t)}{h}\, \chi_h(x_2)\, \boldsymbol{e}_1 \otimes \boldsymbol{e}_2 - \mathcal{C}[\boldsymbol{\alpha}], \end{aligned} \tag{7.1}$$

where χ_h is the indicator function of the layer, q is the signed Burgers content per unit length of the glide plane, and $\gamma(x_1,t) := \int_{-\infty}^{x_1} q(x_1',t)\,\mathrm{d}x_1'$ is the slip, so that $q = \partial_{x_1}\gamma$.

Then $\operatorname{div}\boldsymbol{\alpha} = \mathbf{0}$, and $\operatorname{curl}\boldsymbol{R} = \mathbf{0}$ because $\operatorname{curl}\big((\gamma/h)\,\chi_h\,\boldsymbol{e}_1\otimes\boldsymbol{e}_2\big) = \boldsymbol{\alpha}$ and, by (2.4), $\operatorname{curl}\mathcal{C}[\boldsymbol{\alpha}] = \boldsymbol{\alpha}$.

The plastic distortion $\boldsymbol{\beta}_p = \mathcal{C}[\boldsymbol{\alpha}] + \boldsymbol{R}$ from (2.2) is then the slip on the layer:

$$\boldsymbol{\beta}_p(\boldsymbol{x},t) = \frac{\gamma(x_1,t)}{h}\,\chi_h(x_2)\,\boldsymbol{e}_1\otimes\boldsymbol{e}_2. \tag{7.2}$$

We set $W_R = 0$ without imposing $\boldsymbol{R} = \mathbf{0}$. The energy then depends on $\boldsymbol{R}$ only through $\boldsymbol{\beta}_p$, which is determined by γ, so the evolution of $\boldsymbol{R}$ need not be computed separately (described in (ii) below).

(ii) Transport: For glide, $\boldsymbol{V}_{\boldsymbol{\alpha}} = V(x_1,t)\,\boldsymbol{e}_1$, where V depends on the whole profile $q(\cdot,t)$ and is determined by the Onsager principle (Section 7.B.5), and the transport law (3.7) reduces to

$$\dot q = \partial_{x_1}(qV), \tag{7.3}$$

or, integrating with $\gamma(-\infty,t) = 0$, $\dot\gamma = qV$. We set $\boldsymbol{V}_R = \mathbf{0}$, the limit of vanishing compatible-slip mobility $\boldsymbol{M}_R$, so that $\boldsymbol{R}$ changes only through the compatible slip generated by dislocation motion. Then (3.10) and (3.15) give $\dot{\boldsymbol{\beta}}_p = \boldsymbol{\alpha}\times\boldsymbol{V}_{\boldsymbol{\alpha}} = (qV/h)\,\chi_h\,\boldsymbol{e}_1\otimes\boldsymbol{e}_2$ and $\dot{\boldsymbol{R}} = \mathcal{P}[\dot{\boldsymbol{\beta}}_p]$ the plastic-distortion rate is then that of Kosevich and Mura [Kos62, Mur63]. Hence $\boldsymbol{\beta}_p$ keeps the form (7.2) for all t, and the state is described by γ alone.

(iii) Drag mobility: We take the glide mobility to be $m/|\boldsymbol{\alpha}|$, with $m>0$ constant. The dissipation density $|\boldsymbol{\alpha}|\,|\boldsymbol{V}_{\boldsymbol{\alpha}}|^2/(2m)$ then weights the velocity by the local Burgers content, as in the Wasserstein metric of Section 4, and gives the classical linear drag law for a dislocation line [HL82]. As shown in Section 7.B.5, the velocity then reverses direction where q changes sign: positive and negative Burgers content move in opposite directions under the same stress.

(iv) Initial state: At $t=0$, the density consists of two Gaussian cores of width $\varepsilon \gg h$, centered at $x_1 = \mp d_0/2$:

$$q(x_1,0) = q_0\left[G_\varepsilon\left(x_1+\frac{d_0}{2}\right) - G_\varepsilon\left(x_1-\frac{d_0}{2}\right)\right], \quad \text{where} \quad G_\varepsilon(s) := \frac{1}{\sqrt{2\pi}\varepsilon}\exp\left(-\frac{s^2}{2\varepsilon^2}\right). \tag{7.4}$$

Each core carries Burgers content of magnitude q_0, with opposite signs. For $t>0$, q evolves by (7.3), and the shape and width of the cores change with time. Since the initial state and the loading are symmetric about $x_1=0$, $q(-x_1,t) = -q(x_1,t)$ for all t, and q changes sign at $x_1=0$. Since (7.3) transports q, it preserves the sign of q along particle paths, so $q\ge 0$ for $x_1<0$ and $q\le 0$ for $x_1>0$.

(v) Annihilation: By (iii), the velocity has opposite directions on the two sides of $x_1=0$. When the net stress drives the cores together, positive and negative Burgers content are carried toward $x_1=0$ and cancel there, and the slip $\gamma(0,t)$, which equals the Burgers content on either side of $x_1=0$, decreases to zero. Annihilation thus follows from the transport law. At $x_1=0$, the velocity need not be Lipschitz continuous[4], and (7.3) is understood in the flux form $\dot\gamma = qV$.

7.B. Energies and Evolution Equation

The energy is the free energy (2.15) evaluated on (7.1)–(7.2), up to constants; it is a functional of the slip γ. For each contribution, we give its variational derivative with respect to γ, which determines the driving force.

7.B.1. Elastic Energy

We take isotropic elasticity with shear modulus μ and Poisson's ratio ν. After minimizing out the displacement, the elastic energy of (7.1) is [Pei40, Nab47, HL82]:

$$\mathcal{E}_{\mathrm{el}} := -\frac{K}{2q_0^2}\int_{\mathbb{R}}\int_{\mathbb{R}} q(x_1)\,q(x_1')\,\log|x_1-x_1'|\,\mathrm{d}x_1\,\mathrm{d}x_1', \quad \text{where} \quad K := \frac{\mu q_0^2}{2\pi(1-\nu)}. \tag{7.5}$$

Using $\delta q = \partial_{x_1}\delta\gamma$ and integrating by parts, its variational derivative is

$$\frac{\delta\mathcal{E}_{\mathrm{el}}}{\delta\gamma}(x_1) = \frac{K}{q_0^2}\,\mathrm{p.v.}\int_{\mathbb{R}}\frac{q(x_1')}{x_1-x_1'}\,\mathrm{d}x_1', \tag{7.6}$$

where p.v. denotes the Cauchy principal value.

---

[4] Since a continuous velocity conserves the Burgers vector of every convected circuit, annihilation requires a velocity that is not Lipschitz continuous where opposite-sign Burgers content meets. Alternatively, the opposite-sign Burgers dislocations can be considered as distinct populations of dislocations, each with its own velocity [MZ18].

For two point dislocations with Burgers content $\pm q_0$ at separation d, (7.5) and (7.6) recover the classical energy $K \log d$ and attraction K/d of two coplanar opposite-sign edge dislocations [HL82]. For smooth densities, such as the initial state (7.4), (7.6) is bounded: the cores regularize the interaction.

7.B.2. Core Energy

We take the quadratic defect energy $W_\alpha(\boldsymbol{\alpha}) = \kappa|\boldsymbol{\alpha}|^2/2$, $\kappa \geq 0$. Since $|\boldsymbol{\alpha}|^2 = q^2\chi_h/h^2$,

$$\mathcal{E}_\alpha := \frac{\kappa_h}{2}\int_{\mathbb{R}} q^2 \,\mathrm{d}x_1, \quad \text{where} \quad \kappa_h := \frac{\kappa}{h}, \quad \text{and} \quad \frac{\delta\mathcal{E}_\alpha}{\delta\gamma} = -\kappa_h\,\partial_{x_1} q. \tag{7.7}$$

This contribution penalizes concentrated density and therefore favors spreading of the cores.

7.B.3. Lattice Energy

On the glide layer, (7.2) gives exactly

$$\int_\Omega \Psi(\boldsymbol{\beta}_p)\,\mathrm{d}\Omega = \int_{\mathbb{R}} \psi(\gamma)\,\mathrm{d}x_1, \quad \text{where} \quad \psi(\gamma) := h\,\Psi\left(\frac{\gamma}{h}\,\boldsymbol{e}_1 \otimes \boldsymbol{e}_2\right), \tag{7.8}$$

with $\Psi(\mathbf{0}) = 0$. A slip $\gamma = b_{\mathrm{slip}}$ across the layer is the lattice-equivalent increment $\boldsymbol{S} = (b_{\mathrm{slip}}/h)\,\boldsymbol{e}_1 \otimes \boldsymbol{e}_2$, so the invariance of Ψ assumed in Section 2.C gives $\psi(\gamma + b_{\mathrm{slip}}) = \psi(\gamma)$. We take the simplest such form:

$$\psi(\gamma) = A_\psi \sin^2\left(\frac{\pi\gamma}{b_{\mathrm{slip}}}\right), \qquad A_\psi > 0. \tag{7.9}$$

The lattice-equivalent minima occur at $\gamma = n b_{\mathrm{slip}}$, $n \in \mathbb{Z}$. We take $b_{\mathrm{slip}} = q_0$, so that the slip plateau between sufficiently separated cores approaches a lattice-energy minimum.

The lattice energy and its variational derivative are

$$\mathcal{E}_\psi := \int_{\mathbb{R}} \psi(\gamma)\,\mathrm{d}x_1, \qquad \frac{\delta\mathcal{E}_\psi}{\delta\gamma} = \psi'(\gamma) = \frac{\pi A_\psi}{b_{\mathrm{slip}}}\sin\left(\frac{2\pi\gamma}{b_{\mathrm{slip}}}\right). \tag{7.10}$$

The lattice energy favors narrow cores, since it penalizes slip between its minima, while the elastic energy favors spreading. For an isolated dislocation without defect energy and applied stress, the balance $\delta(\mathcal{E}_{\mathrm{el}} + \mathcal{E}_\psi)/\delta\gamma = 0$ gives the Peierls–Nabarro core [Pei40, Nab47]

$$\gamma(x_1) = q_0\left[\frac{1}{2} + \frac{1}{\pi}\arctan\left(\frac{x_1}{\zeta}\right)\right], \quad \text{where} \quad \zeta := \frac{K}{2\pi A_\psi}, \tag{7.11}$$

so the core half-width ζ is set by the ratio of the elastic and lattice energies.

7.B.4. Applied Stress and Total Energy

A uniform resolved shear stress τ, applied through the boundary tractions, contributes the load term $-\displaystyle\int_\Omega \tau\,(\boldsymbol{\beta}_p)_{12}\,\mathrm{d}\Omega$ [Mur13]:

$$\mathcal{E}_\tau := -\tau\int_{\mathbb{R}} \gamma\,\mathrm{d}x_1, \qquad \frac{\delta\mathcal{E}_\tau}{\delta\gamma} = -\tau. \tag{7.12}$$

7.B.5. Onsager Evolution

The total energy is

$$\mathcal{E}_{\mathrm{tot}} := \mathcal{E}_{\mathrm{el}} + \mathcal{E}_\alpha + \mathcal{E}_\psi + \mathcal{E}_\tau, \tag{7.13}$$

and, by (7.6), (7.7), (7.10), and (7.12),

$$\frac{\delta\mathcal{E}_{\mathrm{tot}}}{\delta\gamma}(x_1) = \frac{K}{q_0^2}\,\mathrm{p.v.}\int_{\mathbb{R}} \frac{q(x_1')}{x_1 - x_1'}\,\mathrm{d}x_1' - \kappa_h\,\partial_{x_1} q + \psi'(\gamma) - \tau. \tag{7.14}$$

With $\dot\gamma = qV$ from (7.3) and assumption (ii), the energy rate is

$$\frac{\mathrm{d}}{\mathrm{d}t}\mathcal{E}_{\mathrm{tot}} = \int_{\mathbb{R}} \frac{\delta\mathcal{E}_{\mathrm{tot}}}{\delta\gamma}\, qV\,\mathrm{d}x_1 = -\int_{\mathbb{R}} fV\,\mathrm{d}x_1, \quad \text{where} \quad f := q\,\tau_{\mathrm{tot}}, \quad \text{and} \quad \tau_{\mathrm{tot}} := -\frac{\delta\mathcal{E}_{\mathrm{tot}}}{\delta\gamma}. \tag{7.15}$$

Here τ_{tot} is the total resolved shear stress on the glide plane: by (7.14), the applied stress τ plus the stresses from the elastic interaction, the core energy, and the lattice energy; and f is the glide force per unit length of the glide plane, which reduces to the Peach–Koehler force [HL82] when only the elastic and applied stresses are retained. Comparing with (4.26), f is the integral of $(\boldsymbol{f}_{\boldsymbol{\alpha}})_1$ across the glide layer. With the drag mobility of assumption (iii), the dissipation density $|\boldsymbol{\alpha}|\,|\boldsymbol{V}_{\boldsymbol{\alpha}}|^2/(2m)$ integrates across the layer to $qV^2/(2m)$ for $x_1 < 0$, where $q \geq 0$ by assumption (iv). By symmetry, the Onsager functional (4.4) is twice

$$\mathcal{J} = \int_{-\infty}^{0} \left(\frac{qV^2}{2m} - fV\right)\mathrm{d}x_1. \tag{7.16}$$

Its stationarity gives $qV/m = f = q\,\tau_{\mathrm{tot}}$, so

$$V = m\,\tau_{\mathrm{tot}}, \qquad x_1 < 0, \tag{7.17}$$

and, by symmetry, $V = -m\,\tau_{\mathrm{tot}}$ for $x_1 > 0$. Positive and negative Burgers content therefore move with the same speed in opposite directions, as in continuum dislocation dynamics with signed densities [MZ18]. Substituting (7.17) into $\dot\gamma = qV$ gives the evolution equation

$$\dot\gamma = -m\,\partial_{x_1}\gamma\,\frac{\delta\mathcal{E}_{\mathrm{tot}}}{\delta\gamma}, \qquad x_1 < 0, \tag{7.18}$$

with $\delta\mathcal{E}_{\mathrm{tot}}/\delta\gamma$ given by (7.14) and $\gamma(-x_1,t) = \gamma(x_1,t)$. The core shapes evolve freely: (7.18) is the continuum evolution (4.29) on the glide layer under assumptions (i)–(iii). It is a nonlocal Hamilton–Jacobi equation for γ; related nonlocal Hamilton–Jacobi systems arise in dislocation-density dynamics [EHF08]. Without the lattice and core energies, (7.18) has the form of the continuum limit of discrete dislocations with annihilation [vMPP22], and the dynamic Peierls–Nabarro model, in which γ instead follows an L^2 gradient flow, converges to discrete dislocation dynamics with annihilation [vMP24]. Here, Peierls–Nabarro cores form and glide under the transport-constrained evolution.

At fixed applied stress, the evolution satisfies

$$\frac{\mathrm{d}}{\mathrm{d}t}\mathcal{E}_{\mathrm{tot}} = -2m\int_{-\infty}^{0} q\left(\frac{\delta\mathcal{E}_{\mathrm{tot}}}{\delta\gamma}\right)^2\mathrm{d}x_1 \leq 0, \tag{7.19}$$

which is the glide-layer form of (4.36). To compare the energetic contributions, we introduce the dimensionless quantities

$$D_0 := \frac{d_0}{\varepsilon}, \qquad \mathit{\Lambda} := \frac{K}{A_\psi\varepsilon}, \qquad \mathit{\Gamma}_\alpha := \frac{\kappa_h q_0^2}{A_\psi\varepsilon^2}, \qquad T := \frac{\tau q_0}{A_\psi}. \tag{7.20}$$

Here D_0 is the normalized initial separation, $\mathit{\Lambda}$ and $\mathit{\Gamma}_\alpha$ measure the elastic and defect contributions relative to the lattice-energy scale, and T is the dimensionless applied stress. By (7.11), $\zeta/\varepsilon = \mathit{\Lambda}/(2\pi)$, so $\mathit{\Lambda}$ also compares the Peierls–Nabarro core width with the initial core width.

We solve (7.18), extended to $x_1 > 0$ by symmetry, numerically on a uniform grid over an interval $[-L, L]$ with $L \gg d_0$. The derivative $\partial_{x_1}\gamma$ is discretized with an upwind scheme for Hamilton–Jacobi equations [OS88]. The elastic term is the exact derivative of the energy (7.5), discretized with the logarithmic kernel averaged over grid cells, so the principal value in (7.6) is not evaluated directly; the convolution over the grid is evaluated exactly with the fast Fourier transform, after zero-padding to at least twice the number of grid points. The explicit time step is small enough for stability, and the computed energy decreases monotonically in all runs.

7.C. Annihilation and Unbinding of a Dislocation Pair

We consider cores for which the lattice energy is large compared with the elastic interaction, so that the Peierls–Nabarro core is much narrower than the initial cores. To isolate the effects of lattice energetics and applied loading, we take a small core energy and use

$$\begin{gathered} q_0 = b_{\mathrm{slip}} = 1, \qquad m = 1, \qquad K = 0.00625, \qquad \kappa_h = 2\times 10^{-6}, \\ \varepsilon = 0.025, \qquad A_\psi = 1, \qquad d_0 = 0.20, \end{gathered} \tag{7.21}$$

so that $\Lambda = 0.25$, $\Gamma_\alpha = 0.0032$, and $D_0 = 8$; the applied stress T is varied. The initial separation of eight Gaussian core widths keeps the initial core overlap negligible; the calibration of such lengths depends on the underlying continuum and atomistic descriptions [CAWB06, Dav20, HSRC20, BBNVdG05]. Then $\zeta/\varepsilon = \Lambda/(2\pi) \approx 0.040$, so $\zeta \approx 0.001$. We solve on $[-1, 1]$ with grid spacing $1.25 \times 10^{-4} \approx \zeta/8$. The scheme converges at first order in the grid spacing: halving it reduces the annihilation time at $T = 0$ by about 2%, and the time extrapolated to zero spacing is 1.59, about 3% less than the value 1.65 on this grid.

Figure 3 summarizes the results at $T = 0$. The cores first sharpen, within $t \approx 0.05$, from the initial Gaussian profiles to nearly the Peierls–Nabarro core (7.11), about 11% wider because of the core energy (Figs. 3a and 3c). They then glide toward each other with this shape until they meet at $x_1 = 0$, where their Burgers content cancels; $\gamma(0, t)$ reaches $q_0/2$ at $t \approx 1.65$. Two point dislocations moving with $V = m\,\tau_{\mathrm{tot}}$ under the attraction K/d meet at $t = q_0 d_0^2/(4mK) = 1.6$, in agreement with the extrapolated time 1.59. This velocity does not depend on the core width; in the dynamic Peierls–Nabarro model, the mobility of a core is instead inversely proportional to the integral of q^2, and hence proportional to its width [GM12]. The energy of an isolated core does not depend on its position, so the continuum lattice energy sets the core width but does not resist core motion, and the elastic attraction is unopposed. The energies (Fig. 3b) show three stages. While the cores form, $\mathcal{E}_{\mathrm{tot}}$ drops rapidly, from 0.088 to 0.036 by $t = 0.05$: the lattice energy decreases from 0.073 to 0.008, while the elastic and core energies increase. While the cores glide, $\mathcal{E}_{\mathrm{tot}}$ decreases slowly, to 0.024 at $t = 1.6$; only the elastic energy changes, since the lattice and core energies of a gliding core are constant. When the cores annihilate, all energies drop rapidly to nearly zero.

An applied stress changes this picture (Fig. 4), where $s(t)$ denotes the distance between the centroids of the positive and negative parts of q. Negative T drives the cores together and speeds up annihilation: for $T = -0.05$, $\gamma(0, t)$ reaches $q_0/2$ at $t \approx 0.83$. Positive T pulls the cores apart. For $T = 0.02$, annihilation is delayed to $t \approx 3.06$; for $T = 0.04$, the cores separate, and s grows to $1.6\,d_0$ by $t = 4$. Bisection on T gives annihilation for $T \le 0.03125$ and unbinding for $T \ge 0.03163$, which a finer grid confirms, so the threshold stress is

$$T_{\mathrm{c}} \approx 0.0314 \approx \frac{\Lambda}{D_0} = 0.03125. \tag{7.22}$$

The right-hand side is the force balance $\tau q_0 = K/d_0$ of two point dislocations at the initial separation. Since $\zeta \ll d_0$, the narrow cores interact as point dislocations, and the threshold is set by the elastic attraction at the initial separation.

Thus, the lattice energy keeps the cores narrow, so they glide as compact Peierls–Nabarro cores and interact as point dislocations. An applied stress then either assists annihilation or, above T_{c}, separates the pair.

Remark 7.1 (Spreading of a single core)**.** When the elastic interaction dominates the lattice energy, a dislocation core spreads instead of staying compact and localized. Consider a single dislocation at zero applied stress, with $q(x_1, 0) = q_0 G_\varepsilon(x_1)$, $K = 1$, and $\kappa_h = 0.10$, and with q_0, b_{slip}, m, ε, and A_ψ as in (7.21), so that $\Lambda = 40$ and $\Gamma_\alpha = 160$. Since $q \ge 0$ on $\mathbb{R}$, (7.17) and (7.18) hold on all of $\mathbb{R}$. The core spreads rapidly (Fig. 5). Its half-width $w := q_0/(\pi \max q)$, which equals ζ for the Peierls–Nabarro core (7.11), grows from $0.8\,\varepsilon$ to $6.7\,\varepsilon$ by $t = 0.1$ and to about $7.6\,\varepsilon$ by $t = 1$, where it has nearly stopped changing. Since $\zeta/\varepsilon = \Lambda/(2\pi) \approx 6.4$, the steady core is about 20% wider than the Peierls–Nabarro core (dashed in Fig. 5), because the core energy also favors spreading. We solve on $[-4, 4]$ with grid spacing $10^{-3} = \varepsilon/25$; doubling the grid spacing or the domain size changes w by less than 0.1%. □

7.D. Relation to Core and Lattice Energetics

The behaviors described above can be placed in relation to existing knowledge of defect, core, and lattice energetics in dislocation theory.

When the defect and lattice energies are retained, the present theory yields a more general thermodynamic driving force. As shown in (4.15), the force on $\boldsymbol{\alpha}$ contains the effective-stress contribution involving $-\dfrac{\partial \Psi}{\partial \boldsymbol{\beta}_p}$, together with the defect contribution involving $-\operatorname{curl} \boldsymbol{P}_\alpha^{\mathrm{d}}$. The former is generated by the nonconvex lattice energy, while the latter is generated by the defect energy W_α. These terms are absent from stress-only Peach–Koehler closures, e.g., [LS06, LS07, LS08, XEA15, MZ18]. However, related energetic contributions are present in other dislocation models. Defect energies and their associated back-stress, diffusion-stress, line-tension, gradient, and curvature contributions have appeared in statistical and thermodynamic continuum dislocation theories [GCZ03, Zai15, Hoc16].

Phase-field dislocation theories have likewise incorporated Peierls-type, generalized stacking-fault, and multiwell lattice energies for crystallographic slip, including atomistically informed energy landscapes that represent lattice resistance and barriers to dislocation motion [KCO02, HBGK11, PMB$^+$20]. Peierls and Frenkel–Kontorova descriptions similarly represent lattice energetics through nonconvex slip potentials and show that lattice discreteness and nonlinearity can strongly influence dislocation kinetics and stability under applied stress [Ros01, RV13]. In Section 7.C, for example, the balance of the elastic and lattice energies selects nearly the Peierls–Nabarro core (7.11), as in these models.

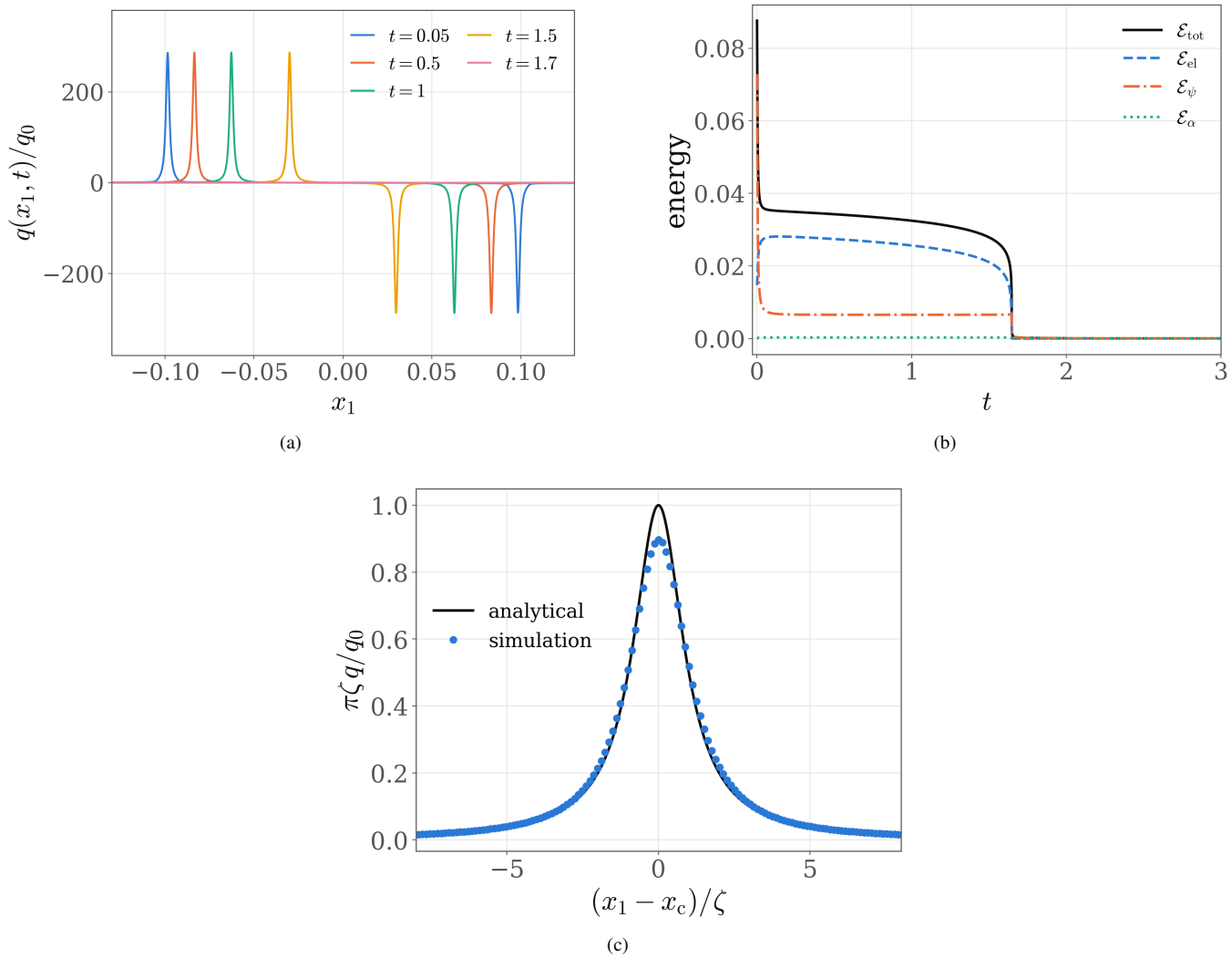


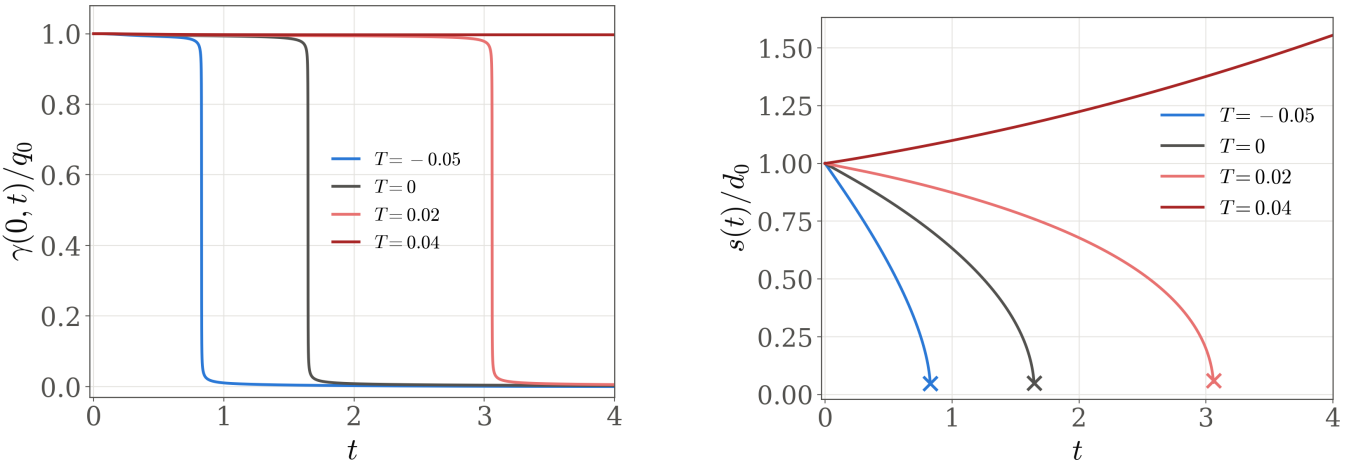
Figure 3. Evolution of an opposite-sign dislocation pair at $T = 0$. **(a)** Signed density $q(x_1, t)$ at several times. By $t = 0.05$, the initial Gaussian cores have sharpened to nearly the Peierls–Nabarro width; they then glide toward each other and annihilate at $x_1 = 0$. **(b)** Elastic, core, lattice, and total energies along the evolution. **(c)** Profile of one core at $t = 0.75$, centered at its maximum x_c, compared with the Peierls–Nabarro core (7.11).

8. Concluding Remarks

We have developed a transport-constrained variational gradient-flow formulation for continuum dislocation evolution. The central idea is that the admissible rates for the gradient flow must be generated by dislocation transport. In the formulation developed here, the plastic distortion is reconstructed from the dislocation density tensor and the compatible slip, with their evolution restricted to the transport directions obtained from geometric conservation principles. The corresponding transport velocities are selected by minimizing a constrained Onsager functional, rather than being introduced independently as a closure such as the Peach–Koehler force. The resulting theory has a formal gradient-flow structure compatible with the geometric dislocation conservation law; it provides the dissipative structure of a gradient flow while enforcing the geometric aspects of dislocation motion.

A key consequence of the gradient flow approach is that the dislocation driving force contains contributions beyond those that arise from elasticity, in contrast to the classical Peach–Koehler force on a dislocation. When the lattice energy and core energy are neglected, the classical Peach–Koehler line force is recovered for a straight dislocation line.

We apply the model to predict the evolution of two opposite-sign dislocations on a single glide layer, where it reduces to one evolution equation for the slip, which we solve numerically. The lattice energy keeps the cores at the Peierls–Nabarro width, and they glide toward each other and annihilate. An applied shear stress either assists annihilation or, above a threshold set by the elastic attraction at the initial separation, separates the pair. The total energy drops rapidly as the cores form and as they annihilate, and slowly as they glide toward each other.



(a) (b)

Figure 4. The dislocation pair under a uniform applied stress T. **(a)** Midpoint slip $\gamma(0,t)$. **(b)** Centroid separation $s(t)$, up to annihilation (crosses, where $\gamma(0,t) = q_0/2$). Negative T speeds up annihilation, small positive T delays it, and $T > T_c \approx 0.031$ separates the pair.

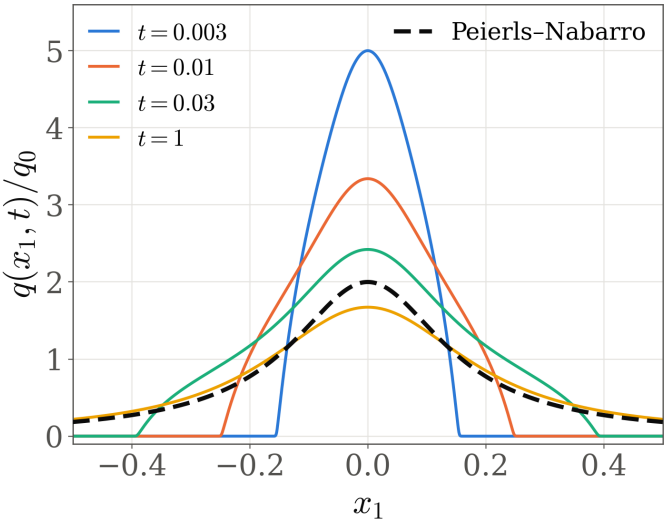


Figure 5. Spreading of a single dislocation core when the elastic interaction dominates (Remark 7.1): signed density $q(x_1,t)$ at several times. The dashed curve is the Peierls–Nabarro core (7.11).

An important unexplored direction is the role of temperature. The kinetics in this paper are athermal: the quadratic dissipation gives a linear force–velocity relation. Unresolved activation barriers could be included through temperature-dependent, nonquadratic dissipation [KAA75, MPR14], which retains a generalized gradient structure. Proposition 4.1 establishes energy decay for time-independent loading, but not convergence to an energy minimum, and the transport constraint may admit additional stationary states; for example, a dislocation-free state remains dislocation-free. A rigorous understanding of the role of thermal effects and the interplay with nonconvexity is an important direction for the future.

Software and Data Availability. The code developed for this work and the associated data are available at `https://github.com/PariaBehnoud/transport-constrained-gradient-flow-dislocations`.

Acknowledgments. We acknowledge John Clayton, Abigail Hunter, David Kinderlehrer, Jaroslaw Knap, Phoebus Rosakis, and Pradeep Sharma for insightful discussions; ARL (W911NF-25-2-0136) and ARO (MURI W911NF-25-2-0164) for financial

support; and NSF-ACCESS (MTH250040) for computing resources provided by the Pittsburgh Supercomputing Center.

[ABDG98] Chérif Amrouche, Christine Bernardi, Monique Dauge, and Vivette Girault. Vector potentials in three-dimensional non-smooth domains. *Mathematical Methods in the Applied Sciences*, 21(9):823–864, 1998.

[AD15a] Vaibhav Agrawal and Kaushik Dayal. A dynamic phase-field model for structural transformations and twinning: Regularized interfaces with transparent prescription of complex kinetics and nucleation. part i: Formulation and one-dimensional characterization. *Journal of the Mechanics and Physics of Solids*, 85:270–290, 2015.

[AD15b] Vaibhav Agrawal and Kaushik Dayal. A dynamic phase-field model for structural transformations and twinning: Regularized interfaces with transparent prescription of complex kinetics and nucleation. part ii: Two-dimensional characterization and boundary kinetics. *Journal of the Mechanics and Physics of Solids*, 85:291–307, 2015.

[AGS08] Luigi Ambrosio, Nicola Gigli, and Giuseppe Savaré. *Gradient Flows: In Metric Spaces and in the Space of Probability Measures*. Birkhäuser, 2008.

[AL17] Eleni Agiasofitou and Markus Lazar. Micromechanics of dislocations in solids: J-, m-, and l-integrals and their fundamental relations. *International Journal of Engineering Science*, 114:16–40, 2017.

[ALGP16] Roberto Alicandro, Lucia De Luca, Adriana Garroni, and Marcello Ponsiglione. Dynamics of discrete screw dislocations on glide directions. *Journal of The Mechanics and Physics of Solids*, 92:87–104, 2016.

[AP99] A Arsenlis and DM Parks. Crystallographic aspects of geometrically-necessary and statistically-stored dislocation density. *Acta materialia*, 47(5):1597–1611, 1999.

[AP02] Athanasios Arsenlis and David M Parks. Modeling the evolution of crystallographic dislocation density in crystal plasticity. *Journal of the Mechanics and Physics of Solids*, 50(9):1979–2009, 2002.

[BBNVdG05] A. A. Benzerga, Y. Bréchet, A. Needleman, and E. Van der Giessen. The stored energy of cold work: Predictions from discrete dislocation plasticity. *Acta Materialia*, 53(18):4765–4779, 2005.

[BFLM15] T. Blass, I. Fonseca, G. Leoni, and M. Morandotti. Dynamics for systems of screw dislocations. *SIAM Journal on Applied Mathematics*, 75(2):393–419, 2015.

[BH16] I. J. Beyerlein and A. Hunter. Understanding dislocation mechanics at the mesoscale using phase field dislocation dynamics. *Philosophical Transactions of the Royal Society A: Mathematical, Physical and Engineering Sciences*, 374(2066):20150166, 2016.

[BS25] P. Behnoud and H. M. Shodja. Ab initio calculation of surface elasticity parameters in cubic crystalline films with surface point defects: Effects on sh wave propagation. *Mechanics of Materials*, 207:105366, 2025.

[BSW01] Ernst Binz, Günter Schwarz, and Jan Wenzelburger. On the dynamics of continuous distributions of dislocations. *Quarterly of Applied Mathematics*, 59(2):225–239, 2001.

[Cah61] John W. Cahn. On spinodal decomposition. *Acta Metallurgica*, 9(9):795–801, 1961.

[CAWB06] Wei Cai, Athanasios Arsenlis, Christopher R. Weinberger, and Vasily V. Bulatov. A non-singular continuum theory of dislocations. *Journal of the Mechanics and Physics of Solids*, 54(3):561–587, 2006.

[CCP+13] Yong S. Chen, Woosong Choi, Stefanos Papanikolaou, Matthew Bierbaum, and James P. Sethna. Scaling theory of continuum dislocation dynamics in three dimensions: Self-organized fractal pattern formation. *International Journal of Plasticity*, 46:94–129, 2013.

[CCS+10] Zi Chen, Kevin T. Chu, David J. Srolovitz, Jeffrey M. Rickman, and Mikko P. Haataja. Dislocation climb strengthening in systems with immobile obstacles: Three-dimensional level-set simulation study. *Physical Review B*, 81(5):054104, February 2010.

[CG99] Paolo Cermelli and Morton E. Gurtin. The motion of screw dislocations in crystalline materials undergoing antiplane shear: Glide, cross-slip, fine cross-slip. *Archive for Rational Mechanics and Analysis*, 148:3–52, 1999.

[CH58] John W. Cahn and John E. Hilliard. Free energy of a nonuniform system. i. interfacial free energy. *The Journal of Chemical Physics*, 28(2):258–267, 02 1958.

[Cla11] John D Clayton. *Nonlinear mechanics of crystals*, volume 616. Springer Dordrecht, 2011.

[Cla15] JD Clayton. Defects in nonlinear elastic crystals: differential geometry, finite kinematics, and second-order analytical solutions. *ZAMM-Journal of Applied Mathematics and Mechanics/Zeitschrift für Angewandte Mathematik und Mechanik*, 95(5):476–510, 2015.

[CTC97] W. Craig Carter, J. E. Taylor, and J. W. Cahn. Variational methods for microstructural-evolution theories. *JOM*, 49(12):30–36, 1997.

[Dav20] Kamyar M. Davoudi. Core energy and regularization parameters of non-singular continuum theories of dislocations using atomistic simulations, 2020.

[DKW18] Patrick W. Dondl, Matthias W. Kurzke, and Stephan Wojtowytsch. The effect of forest dislocations on the evolution of a phase-field model for plastic slip. *Archive for Rational Mechanics and Analysis*, 232(1):65–119, oct 2018.

[Doi11] Masao Doi. Onsager's variational principle in soft matter. *Journal of Physics: Condensed Matter*, 23(28):284118, jun 2011.

[EAP20] Anter El-Azab and Giacomo Po. Continuum dislocation dynamics: Classical theory and contemporary models. In Wanda Andreoni and Sidney Yip, editors, *Handbook of Materials Modeling: Methods: Theory and Modeling*, pages 1583–1607. Springer International Publishing, Cham, 2020.

[EE07] Marcelo Epstein and Marek Elżanowski. *Material Inhomogeneities and their Evolution: A Geometric Approach*. Springer, 2007.

[EHF08] Ahmad El Hajj and Nicolas Forcadel. A convergent scheme for a non-local coupled system modelling dislocations densities dynamics. *Mathematics of Computation*, 77(262):789–812, 2008.

[Eri80] J. L. Ericksen. Some phase transitions in crystals. *Archive for Rational Mechanics and Analysis*, 73(2):99–124, 1980.

[Fri24] Gero Friesecke. *Optimal Transport: A Comprehensive Introduction to Modeling, Analysis, Simulation, Applications*. Society for Industrial and Applied Mathematics, Philadelphia, PA, 2024.

[GB99] I. Groma and P. Balogh. Investigation of dislocation pattern formation in a two-dimensional self-consistent field approximation. *Acta Materialia*, 47(13):3647–3654, 1999.

[GCZ03] I. Groma, F. F. Csikor, and M. Zaiser. Spatial correlations and higher-order gradient terms in a continuum description of dislocation dynamics. *Acta Materialia*, 51(5):1271–1281, 2003.

[GH03] Huajian Gao and Yonggang Huang. Geometrically necessary dislocation and size-dependent plasticity. *Scripta Materialia*, 48(2):113–118, 2003.

[GM12] María del Mar González and Régis Monneau. Slow motion of particle systems as a limit of a reaction-diffusion equation with half-Laplacian in dimension one. *Discrete and Continuous Dynamical Systems*, 32(4):1255–1286, 2012.

[Gur04] Morton E. Gurtin. A gradient theory of small-deformation isotropic plasticity that accounts for the burgers vector and for dissipation due to plastic spin. *Journal of the Mechanics and Physics of Solids*, 52(11):2545–2568, 2004.

[HBGK11] A. Hunter, I. J. Beyerlein, T. C. Germann, and M. Koslowski. Influence of the stacking fault energy surface on partial dislocations in FCC metals with a three-dimensional phase field dislocation dynamics model. *Physical Review B*, 84(14):144108, 2011.

[HL82] John P. Hirth and Jens Lothe. *Theory of Dislocations*. Wiley, New York, 2nd edition, 1982.

[Hoc16] Thomas Hochrainer. Thermodynamically consistent continuum dislocation dynamics. *Journal of the Mechanics and Physics of Solids*, 88:12–22, 2016.

[HSRC20] Yi Hu, B. A. Szajewski, D. Rodney, and W. A. Curtin. Atomistic dislocation core energies and calibration of non-singular discrete dislocation dynamics. *Modelling and Simulation in Materials Science and Engineering*, 28(1):015005, 2020.

[HSZG14] Thomas Hochrainer, Stefan Sandfeld, Michael Zaiser, and Peter Gumbsch. Continuum dislocation dynamics: towards a physical theory of crystal plasticity. *Journal of the Mechanics and Physics of Solids*, 63:167–178, 2014.

[HZG07] T. Hochrainer, M. Zaiser, and P. Gumbsch. A three-dimensional continuum theory of dislocation systems: kinematics and mean-field formulation. *Philosophical Magazine*, 87(8-9):1261–1282, 2007.

[JKO98] Richard Jordan, David Kinderlehrer, and Felix Otto. The variational formulation of the fokker–planck equation. *SIAM Journal on Mathematical Analysis*, 29(1):1–17, 1998.

[KAA75] U. F. Kocks, A. S. Argon, and M. F. Ashby. *Thermodynamics and Kinetics of Slip*, volume 19 of *Progress in Materials Science*. Pergamon Press, 1975.

[KCO02] M. Koslowski, A. M. Cuitiño, and M. Ortiz. A phase-field theory of dislocation dynamics, strain hardening and hysteresis in ductile single crystals. *Journal of the Mechanics and Physics of Solids*, 50(12):2597–2635, 2002.

[KL01] David Kinderlehrer and Chun Liu. Evolution of grain boundaries. *Mathematical Models and Methods in Applied Sciences*, 11:713–729, 06 2001.

[KLL+04] D. Kinderlehrer, Jason Lee, Irene Livshits, A.D. Rollett, and Shlomo Ta'asan. Mesoscale simulation of grain growth. *Materials Science Forum*, 467-470:1057–1062, 10 2004.

[KLT04] Marisol Koslowski, Richard LeSar, and Robb Thomson. Dislocation structures and the deformation of materials. *Phys. Rev. Lett.*, 93:265503, Dec 2004.

[KOPF20] O. Kolednik, W. Ochensberger, J. Predan, and F. D. Fischer. Driving forces on dislocations – an analytical and finite element study. *International Journal of Solids and Structures*, 190:181–198, 2020.

[Kos62] A. M. Kosevich. The deformation field in an isotropic elastic medium containing moving dislocations. *Soviet Physics JETP*, 15(1):108–115, 1962. English translation of Zh. Eksp. Teor. Fiz. 42, 152–162 (1962).

[Krö58] Ekkehart Kröner. *Kontinuumstheorie der Versetzungen und Eigenspannungen*, volume 5 of *Ergebnisse der angewandten Mathematik*. Springer, Berlin, 1958.

[Krö10] Ekkehart Kröner. General continuum theory of dislocations and proper stresses. `http://neo-classical-physics.info`, 2010. English translation of the original 1958 German text "Kontinuumstheorie der Versetzungen und Eigenspannungen".

[Laz13] Markus Lazar. The fundamentals of non-singular dislocations in the theory of gradient elasticity: Dislocation loops and straight dislocations. *International Journal of Solids and Structures*, 50(2):352–362, 2013.

[LeS14] Richard LeSar. Simulations of dislocation structure and response. *Annual Review of Condensed Matter Physics*, 5:375–407, 03 2014.

[LM05] Markus Lazar and Gérard A Maugin. Nonsingular stress and strain fields of dislocations and disclinations in first strain gradient elasticity. *International journal of engineering science*, 43(13-14):1157–1184, 2005.

[LS06] Surachate Limkumnerd and James P. Sethna. Mesoscale theory of grains and cells: Crystal plasticity and coarsening. *Phys. Rev. Lett.*, 96:095503, Mar 2006.

[LS07] Surachate Limkumnerd and James P. Sethna. Stress-free states of continuum dislocation fields: Rotations, grain boundaries, and the nye dislocation density tensor. *Phys. Rev. B*, 75:224121, Jun 2007.

[LS08] S. Limkumnerd and J. P. Sethna. Shocks and slip systems: Predictions from a mesoscale theory of continuum dislocation dynamics. *Journal of the Mechanics and Physics of Solids*, 56(4):1450–1459, 2008.

[McD24] David L McDowell. Nonequilibrium statistical thermodynamics of thermally activated dislocation ensembles: part 1: subsystem reactions under constrained local equilibrium. *Journal of Materials Science*, 59(12):5093–5125, 2024.

[MO08] Alexander Mielke and Michael Ortiz. A class of minimum principles for characterizing the trajectories and the relaxation of dissipative systems. *ESAIM: Control, Optimisation and Calculus of Variations*, 14(3):494–516, 2008.

[MPR14] Alexander Mielke, Mark A. Peletier, and D. R. Michiel Renger. On the relation between gradient flows and the large-deviation principle, with applications to Markov chains and diffusion. *Potential Analysis*, 41(4):1293–1327, 2014.

[Mur63] T Mura. Continuous distribution of moving dislocations. *Philosophical Magazine*, 8(89):843–857, 1963.

[Mur13] Toshio Mura. *Micromechanics of defects in solids*. Springer Science & Business Media, 2013.

[MZ18] Mehran Monavari and Michael Zaiser. Annihilation and sources in continuum dislocation dynamics. *Materials Theory*, 2(1):3, 2018.

[Nab47] F. R. N. Nabarro. Dislocations in a simple cubic lattice. *Proceedings of the Physical Society*, 59(2):256–272, 1947.

[Ons31] Lars Onsager. Reciprocal relations in irreversible processes. i. *Phys. Rev.*, 37:405–426, Feb 1931.

[OS88] Stanley Osher and James A. Sethian. Fronts propagating with curvature-dependent speed: Algorithms based on Hamilton–Jacobi formulations. *Journal of Computational Physics*, 79(1):12–49, 1988.

[Ott01] Felix Otto. The geometry of dissipative evolution equations: The porous medium equation. *Communications in Partial Differential Equations*, 26(1–2):101–174, 2001.

[Pei40] R. Peierls. The size of a dislocation. *Proceedings of the Physical Society*, 52(1):34–37, 1940.

[PF90] Oliver Penrose and Paul C. Fife. Thermodynamically consistent models of phase-field type for the kinetic of phase transitions. *Physica D: Nonlinear Phenomena*, 43(1):44–62, 1990.

[PLAG18] Giacomo Po, Markus Lazar, Nikhil Chandra Admal, and Nasr Ghoniem. A non-singular theory of dislocations in anisotropic crystals. *International Journal of Plasticity*, 103:1–22, 2018.

[PMB+20] Xiaoyao Peng, Nithin Mathew, Irene J. Beyerlein, Kaushik Dayal, and Abigail Hunter. A 3d phase field dislocation dynamics model for body-centered cubic crystals. *Computational Materials Science*, 171:109217, 2020.

[PZ03] Mario Pitteri and Giovanni Zanzotto. *Continuum Models for Phase Transitions and Twinning in Crystals*. Chapman and Hall/CRC, 2003.

[RLBF03] David Rodney, Yann Le Bouar, and Alphonse Finel. Phase field methods and dislocations. *Acta Materialia*, 51(1):17–30, 2003.

[Ros01] Phoebus Rosakis. Supersonic dislocation kinetics from an augmented peierls model. *Phys. Rev. Lett.*, 86:95–98, Jan 2001.

[RV97] J. M. Rickman and Jorge Viñals. Modelling of dislocation structures in materials. *Philosophical Magazine A*, 75(5):1251–1262, May 1997.

[RV13] Phoebus Rosakis and Anna Vainchtein. New solutions for slow moving kinks in a forced frenkel–kontorova chain. *Journal of Nonlinear Science*, 23(6):1089–1110, 2013.

[San15] Filippo Santambrogio. *Optimal Transport for Applied Mathematicians*. Birkhäuser, 2015.

[San17] Filippo Santambrogio. Euclidean, metric, and wasserstein gradient flows: an overview. *Bulletin of Mathematical Sciences*, 7(1):87–154, 2017.

[SW04] Chen Shen and Yunzhi Wang. Incorporation of γ-surface to phase field model of dislocations: Simulating dislocation dissociation in FCC crystals. *Acta Materialia*, 52(3):683–691, 2004.

[SY23] Fabio Sozio and Arash Yavari. A geometric field theory of dislocation mechanics. *Journal of Nonlinear Science*, 33:83, 2023.

[SZ15] Stefan Sandfeld and Michael Zaiser. Pattern formation in a minimal model of continuum dislocation plasticity. *Modelling and Simulation in Materials Science and Engineering*, 23(6):065005, jul 2015.

[vMP24] Patrick van Meurs and Stefania Patrizi. Discrete dislocation dynamics with annihilation as the limit of the Peierls–Nabarro model in one dimension. *SIAM Journal on Mathematical Analysis*, 56(1):197–233, 2024.

[vMPP22] Patrick van Meurs, Mark A. Peletier, and Norbert Požár. Discrete-to-continuum convergence of charged particles in 1D with annihilation. *Archive for Rational Mechanics and Analysis*, 246(1):241–297, 2022.

[Wen98] Jan Wenzelburger. A kinematic model for continuous distributions of dislocations. *Journal of Geometry and Physics*, 24(4):334–352, 1998.

[WJCK01] Yu U. Wang, Y. M. Jin, Alberto M. Cuitiño, and Armen G. Khachaturyan. Nanoscale phase field microelasticity theory of dislocations: Model and three-dimensional simulations. *Acta Materialia*, 49(10):1847–1857, 2001.

[XEA15] Shengxu Xia and Anter El-Azab. Computational modelling of mesoscale dislocation patterning and plastic deformation of single crystals. *Modelling and Simulation in Materials Science and Engineering*, 23(5):055009, may 2015.

[Yav13] Arash Yavari. Compatibility equations of nonlinear elasticity for non-simply-connected bodies. *Archive for Rational Mechanics and Analysis*, 209:237–253, 2013.

[YG12] Arash Yavari and Alain Goriely. Riemann–Cartan geometry of nonlinear dislocation mechanics. *Archive for Rational Mechanics and Analysis*, 205:59–118, 2012.

[Zai15] Michael Zaiser. Local density approximation for the energy functional of three-dimensional dislocation systems. *Physical Review B*, 92(17):174120, 2015.

[ZWZ25] Yufan Zhang, Ronghai Wu, and Michael Zaiser. Continuum dislocation dynamics as a phase field theory with conserved order parameters: formulation and application to dislocation patterning. *Modelling and Simulation in Materials Science and Engineering*, 33(3):035011, 03 2025.